

Erlend Salte Kallelid

Evolution in Cosmic Noise Absorption During Periodic Events

Master's thesis in MLREAL

Supervisor: Noora Partamies and Patrick Espy

December 2019

Erlend Salte Kallelid

Evolution in Cosmic Noise Absorption During Periodic Events

Master's thesis in MLREAL
Supervisor: Noora Partamies and Patrick Espy
December 2019

Norwegian University of Science and Technology
Faculty of Information Technology and Electrical Engineering
Department of Physics



Preface

This is my master's thesis that marks that my five years long master teaching program at NTNU is going towards the end. The program consists of four years of physics and mathematics and one year of pedagogic, of which half an year remains. I am very happy to have been given the chance to spend one full year at the University Centre in Svalbard (UNIS). Here I have learned a lot about space physics, which I can use both inside and outside of school.

The purpose of this study was to examine how the ionosphere responds to intense substorms and energetic electron precipitation. Events lasting for longer time, preferable many days were of special interest. In order to do so, data from three riometers and five magnetometers from a six years long period have been analysed. The subject has not been looked much into before. The work presented in this paper, is therefore most important for suggesting what should be the focus in more comprehensive studies in the future.

Acknowledgements

First of all I want to thank Noora Partamies for being the best supervisor a student can dream of. I have always felt welcome when I have dropped by to ask for questions. She never gave any impression of not having time to explain in detail the subjects that were unclear to me. Furthermore she proofread my thesis in detail and gave insightful feedbacks

I also want to thank Lidia Luque and Markus Floer, whom I have shared office with the last months. They have also been good partners to discuss certain details with. I also want to thank Patrick Espy for suggesting that I should go to Svalbard in the first place. He was the one that inspired me to study atmospheric physics.

Finally, I want to thank family and friends for their company and moral support, which I have valued immensely.

Summary

The evolution of energetic electron precipitation in the ionosphere above Lapland was examined by using 5 magnetometers and 3 riometers in the period from 2008 to 2013. The magnetometers gave rise to the IL index, which defined the phases and the intensity of the substorms. The amount of cosmic noise absorption was evaluated with respect to the substorm intensity. During this 6-year period, 245 events were evaluated. 79 of them occurred as single night events, while the remaining 166 came in groups of at least 2 nights in a row. The substorms were classified into intensity categories of either -400, -600 or -800 nT.

The single night events were divided into isolated and compound substorms, depending on the number of expansion and recovery phases. Each event night in the multi-night events was evaluated from the first expansion phase to the last recovery phase. The event nights had an average duration of about 8 ± 3 hours around midnight, which is the time sector where the IL index records at least 80 % of the global magnetic activity. This makes the IL index a good reference for co-located riometers, even for these very long event nights.

A linear correlation between cosmic noise absorption and substorm intensity was found when averaging from start to end of each event night. However, this linearity breaks down when the events are examined in detail. Relative to the strength of the magnetic disturbance, there seems to be a higher cosmic noise absorption in the late night and early morning sector. This is especially important for the events with the most intense substorms.

During multi-night events, the cosmic noise absorption often showed higher values for the second to fourth night. This behaviour can also be caused by external factors like the solar wind and geomagnetic storms. Thus, the Dst index and solar wind data should be included in future studies.

Finally, these substorm events are associated with electron precipitation with high enough energy to ionise neutral species in the atmosphere. Earlier studies have shown that such events can alter the atmospheric chemistry on a short term scale. The occurrence rate of such events is so high, that the precipitation may be a significant player in atmospheric chemistry.

Table of Contents

Preface	1
Summary	i
Table of Contents	iv
List of Figures	vii
1 Introduction	1
1.1 Background	1
1.2 Scientific motivation	2
2 Literature Review	3
2.1 Substorm phases	3
2.2 Substorm duration and phase pairs	4
2.3 Energy input	4
2.4 Particle precipitation during substorms	5
3 Data and instruments	7
3.1 Cosmic noise absorption and riometers	8
3.2 IL index	9
3.3 Categories of substorms and periodic events	10
4 Experiment / Results	17
4.1 Correlation between substorm intensity and cosmic noise absorption	17
4.2 Events lasting for 2 to 3 nights	19
4.3 Events lasting for 4 or more nights	19
4.4 Compound substorms	22
4.5 Timing of phase pairs	24

5	Example event: 10-12th July 2013	27
5.1	An intense triple compound substorm	27
5.2	Two compound substorms	31
6	Discussion	35
6.1	Local effects	35
6.2	Phase pairs	36
6.3	Substorm intensity and timing of phase pairs	37
6.4	Multi-night events	38
6.5	Compound substorms	39
6.6	Atmospheric effects	40
7	Conclusion	41
	Bibliography	43

List of Figures

3.1	The map shows the stations used for the study. They are marked with orange and yellow. The red dots are magnetometers in the IMAGE network.	7
3.2	The figure shows the absorption during a -400 nT substorm. The blue, red and yellow lines represent the absorption A_{dB} at the stations of Abisko, Ivalo and Sodankylä, respectively. The thick black line is the upper envelope curve. The green, red and blue shadings represent the growth, expansion and recovery phase, respectively.	9
3.3	The figures show two consecutive days before they were separated into event nights.	11
3.4	The figure shows a schematic representation of the event types. All of them are also separated into -400, -600 or -800 nT event nights.	12
3.5	The figures shows an isolated -400 nT substorm during an single night. The top panel shows the IL index whereas the bottom panel shows the CNA.	13
3.6	The figures shows a compound -400 nT substorm during an single night. The top panel shows the IL index whereas the bottom panel shows the CNA.	14
3.7	The figures shows a -400 nT 2 night event. The top panel shows the IL index whereas the bottom panel shows the CNA.	15
3.8	The figures shows an -400 nT 7-night event. The top panel shows the IL index whereas the bottom panel shows the CNA.	16
4.1	The figure shows the median of the CNA rate for all the event types and intensities.	18
4.2	The figure shows the median of the total CNA for all the event types and intensities.	18
4.3	The figure shows the CNA rate for the events lasting for 2-3 nights for the three intensity classes. It shows how the CNA rate develops from night 1 to 2, and 3 if existed. Each coloured line represents a different event whereas the black line gives the median CNA rate value per night.	20

4.4	The figure shows the total CNA for the events lasting for 2-3 nights for the three intensity classes. It shows how the total CNA develops from night 1 to 2, and 3 if existed. Each coloured line represents a different event whereas the black line gives the median CNA rate value per night.	20
4.5	The figure shows the CNA rate for the events lasting for 4 nights or more for the three intensity classes. It shows how the CNA rate develops from one night to another. Each coloured line represents a different event whereas the black line gives the median of the first night, then second night and so on.	21
4.6	The figure shows the total CNA for the events lasting for 4 nights or more for the three intensity classes. It shows how the total CNA develops from one night to another. Each coloured line represents a different event whereas the black line gives the median of the first night, then second night and so on.	21
4.7	The vertical blue error bars represent the total CNA for each phase pair and the total CNA of the entire substorm (the first bar). They include 1 standard deviation. The red curve marks a halving of CNA rate. There are 226 evaluated nights. The purple line (at 300 dB) is the median CNA rate for all the nights. The yellow curve shows the median absorption rate for all of the phase pairs. Note that the yellow and purple curves have been multiplied by 500 to allow the curves to be plotted in the same figure. . .	22
4.8	The figure shows the median duration and one standard deviation for the five longest phase pairs for all the 226 nights.	23
4.9	The figure shows how often the most, second most and third most absorbing phase pair occurs as the phase pair number 1-11 for the 226 evaluated nights.	25
4.10	The figure shows the same as figure 4.9, but now the 226 event nights are separated into the intensity categories of -400, -600 and -800 nT, resulting in 96, 85 and 45 events, respectively.	26
5.1	The figure shows Dst index (nT). The two black bars mark the periods of events being analysed.	28
5.2	The figure shows the IL index. The horizontal lines marks the ± 100 nT for the -800 nT category. The numbered arrows at the top indicate the phase pairs.	28
5.3	The figure shows the CNA. The numbered arrows at the top indicate the phase pairs.	29
5.4	The bars show the total CNA and the duration for each phase pair. The yellow line shows the CNA rate per phase pair and the black line shows the CNA rate for the entire event. Note that the CNA rates have been multiplied by 100 to allow them to be plotted in the same figure.	29
5.5	The top panel shows the energy input ϵ (W) and the bottom panel shows the IMF B_z measured by the ACE satellite. The times on the x-axis are shifted such that they show when the IMF reaches the magnetopause. The time shift is calculated from the solar wind bulk speed of 440 km/s. . . .	30

5.6	The figure shows the electron density (m^{-3}) measured by EISCAT VHF. The radar was pointing in the field aligned direction. The red and blue bars at the top mark the 5 phase pairs.	30
5.7	The figure shows the IL index. The horizontal lines marks the ± 100 nT for the -800 nT category. The numbered arrows at the top indicate the phase pairs.	31
5.8	The figure shows the CNA. The numbered arrows at the top indicate the phase pairs.	32
5.9	The bars show the total CNA and the duration for each phase pair. The yellow line shows the CNA rate per phase pair and the black line shows the CNA rate for the entire event. Note that the CNA rates have been multiplied by 100 to allow them to be plotted in the same figure.	32
5.10	The top panel shows the energy input ϵ (W) and the bottom panel shows the IMF B_z measured by the ACE satellite. The times on the x-axis are shifted such that they show when the IMF reaches the magnetopause. The time shift is calculated from the solar wind bulk speed of 430 km/s.	33
5.11	The figure shows the electron density (m^{-3}) measured by EISCAT VHF. The radar was pointing in the field aligned direction. The red and blue bars at the top mark the 4 phase pairs.	33

Introduction

1.1 Background

Northern lights have been a subject for wonder and investigation for many hundreds of years. Already in 1733 the French astronomer de Mairan proposed the idea of aurora being caused by interaction between the Sun and the Earth. Despite the early proposal, it took almost 200 years before the Norwegian scientist Birkeland, in the beginning of 20th century, explained the northern lights as a result of cathode rays (electrons) originating from the Sun. He suggested them being trapped by the Earth's magnetic field, before being absorbed by molecules in the atmosphere, which again emitted the light (Brekke, 1997). Chapman was, in 1962, the first person to name this magnetic activity for substorms. In the following years, the substorms were divided into growth, expansion and recovery phases (McPherron and Chu, 2016). Today we know that the northern lights are only a small part of a very complex system. Some of the processes occur less than 100 kilometers above our heads. But these processes must be understood in light of mechanisms taking place further away than the Moon.

Today we know that substorms are typically associated with energetic electron precipitation (EEP), which has become subject for many recent studies. We know that EEP is able to reach down to the heights of 60-90 km where the interactions between charged and neutral particles are important. Such precipitation is mainly associated with intense substorms with $AL < -400$ nT. Riometers can be used to monitor the electron density (i.e. ionisation) at this altitude, by measuring cosmic noise absorption (CNA). In this study magnetometers are used for defining the phases and intensity of substorms and riometers for determining the CNA. The substorms intensity is defined as the magnetic deflection.

1.2 Scientific motivation

The temporal extent of intense substorms is not very well known. It is also not well understood how much CNA one can expect from such substorms. It is especially interesting to examine how the CNA responds to the periods of multiple substorms. All this will make the basis for this thesis. The study has two different focus areas. In the first part, it is examined whether there exists a correlation between the CNA values of consecutive nights, and whether one can expect more CNA for multi-night events than for single night events. In the second part, the CNA is analysed in light of the substorm intensity. Is it possible to predict the CNA by looking at the substorm intensity? How does the CNA respond to substorms that consists of many expansion phases? Finally, the occurrence rate of these signatures will be discussed. At the moment, there is a standards EEP forcing that goes into the atmospheric chemistry and climate models. But it is an estimate that is based on magnetic indices. It is therefore of interest to understand better to which degree the CNA correlates with the substorm intensity.

Substorm studies are often either case studies of relatively simple substorms. They are easier to analyse and understand in detail. Or statistical approaches are used to examine substorms on a global scale. This study will have one foot in both camps. The data set is not large enough to make proper statistics, but it is too big to analyse every event in detail. The results show some trends. In the end, suggestions for what to focus on in future studies, are given.

Literature Review

2.1 Substorm phases

Today we know that substorms are associated with a negative B_z (geocentric solar magnetospheric (GSM) coordinate system in the interplanetary magnetic field (IMF). This allows for dayside reconnection between the Earth's closed field lines and the IMF, with the result of open terrestrial field convecting over the region with open magnetic field to the night-side (Dungey, 1961; Cowley, 1982). The return convection, back to the dayside, happens outside this region and closes the so called Dungey cycle.

The auroral electrojet (AE), was introduced by Davis and Sugiura (1966). It is driven by the ionospheric convection and large-scale horizontal currents. The ionospheric plasma is frozen-in and moves through the atmosphere together with the magnetic field. In the ionospheric E layer (~ 125 km), the collision rate between positive ions and neutrals is much higher than that of the electrons and neutrals. Consequently, a current, called the auroral electrojet, with an opposite direction to the plasma flow arises. In the dusk region, the current is eastward and in the dawn region, it is westward (Cowley, 2000). Below the westward current, the horizontal component of the magnetic field decreases, forming a so called magnetic bay. The magnitude of the bay is called the auroral lower (AL) index and determines the intensity of the substorm. A similar logic is followed for eastward current, but a hump is formed instead of a bay. The magnitude is called the auroral upper (AU) index and the difference between AU and AL is called the AE index.

By measuring an increased in the AE, McPherron (1970) argued for the existence of a growth phase. It marks the beginning of the substorm and takes place prior the expansion and recovery phase (Akasofu, 1964). It starts with B_z turning negative, magnetic field convecting to the nightside and accumulation of open magnetic field. Consequently, the field lines stretches in the magnetotail, and energy is stored as magnetic flux (McPherron et al., 1973; Siscoe and Huan, 1985).

Finally, at the onset of the expansion phase, energy is released rapidly by the nightside reconnection. The configuration of the magnetic field become more depolarised. The tail field lines map down into the ionosphere with the result of field-aligned currents and

particle precipitation. During the expansion phase the ionospheric activity region expands eastward, westward and poleward, and inside the expanding bulge, an intense westward current can easily be detected by magnetometers (Akasofu, 1964) as the AL index. The peak in AL (maximum deflection of the bay) marks the start of the recovery phase. The AL subsides and the magnetosphere returns to its original undisturbed state (Wing et al., 2013), unless it develops into new expansion phases.

2.2 Substorm duration and phase pairs

The duration of substorms and their phases has been evaluated in multiple studies. The results depend on how the phases are defined and the intensity of the substorm. Tanskanen (2002) and Huang et al. (2003) reported on a total duration of 2-4 hours. Partamies et al. (2013), on the other hand, reported growth, expansion and recovery phases with a median of 31, 12 and 31 minutes, respectively. This sums up to less than 1.5 hours of total duration, but this study used an automatic phase detection algorithm which is very sensitive for new expansion phases in the middle of recovery phases. This results in more and shorter phases. Kullen and Karlsson (2004) combined the expansion and recovery phases. They found less intense substorms ($AE < 300$ nT) to last for 1.3 hours on average and intense substorms ($AE > 300$ nT) to last for 2.3 hours and up to 4-5 hours.

During a substorm, it is common to observe multiple phase pairs, where one phase pair consists of one expansion phase and one recovery phase. Sandhu et al. (2018) defined isolated substorms as substorm with one growth phase, one expansion phase and one recovery phase. In contrast, compound substorms were defined as substorms where (at least) the first recovery phase leads directly into a new expansion phase. Similar, criteria were used by e.g. Huang et al. (2003); Kim et al. (2008); Liou et al. (2013); Newell and Gjerloev (2011); Pulkkinen et al. (2007). Compound substorms are in general less explosive in their nature and they have recurrence rates of 2-3 hours. This is on the the scale of the lifetime of the substorms described earlier. They are often associated with geomagnetic storms and a southward turned IMF or correlation between phase shifts and pulses in the solar wind. Partamies et al. (2013) concluded that compound substorms can last for very long time, easily more than 6 hours. They also concluded that the compound substorms are 10 % more intense than isolated substorms. In the study of Sandhu et al. (2018), compound substorms were found to be driven by high coupling rate between the solar wind and magnetosphere, which in the end, resulted in more intense substorms because of increased energy content in the ring current (the equatorial current in the near-Earth space).

2.3 Energy input

In order to examine the total available energy in the magnetosphere, it is common to use Akasofu's epsilon parameter (Perreault and Akasofu, 1978) in SI units (Tanskanen, 2002). It gives the energy input from the solar wind:

$$\epsilon(W) = 10^7 \cdot v(m/s) B^2(T) \sin^4(\theta/2) \cdot l_0^2(m) \quad (2.1)$$

where B is the magnitude of IMF (GSM coordinates), θ is the IMF clock angle ($\tan(\theta) = B_y/B_z$), v is the solar wind speed and l_0 an empirical parameter, which is often interpreted as the effective cross-sectional area of interaction between the solar wind and the magnetosphere. For this study, the original value of 7 Re (Akasofu, 1981) is used. However, Tanskanen (2002) suggests a revision to 9-10 Re. They also found an energy input at the order of 2×10^{11} W to be a reasonable threshold for development of substorms.

The traditional loading-unloading model says that the energy for the inner magnetospheric processes comes from the lobes that have been loaded during the growth phase. (McPherron et al., 1973). In contrast, the directly driven model says that the substorm intensity depends on the energy available during the expansion phase. Baker et al. (1996) points out that both scenarios are important. However, Kallio et al. (2000) calculated that the energy input during growth phase is of similar magnitude, regardless of the intensity of the substorm.

2.4 Particle precipitation during substorms

As described above, the dipolarisation processes during expansion phases, are associated with acceleration of particle injections into the ionosphere along the field lines. The details of how this happens is still debated (Reeves et al., 2009). The energies of the precipitating particles range from 20 to 300 keV for typical substorms, but can also reach 1 MeV (Baker et al., 1979). This energetic electron precipitation (EEP) penetrates down to altitudes of 60-90 km (Turunen et al., 2009), i.e. into the D region, and causes strong ionisation. For comparison, electron precipitation with energies of 1-10 keV are deposited above 100 km, and causes the aurora (Oyama et al., 2017).

For a typical substorm, the EEP area range from 62-75° latitude, but peaks at 68° (Cresswell-Moorcock et al., 2013). The EEP initially starts in this region around magnetic midnight. Elphinstone et al. (1995) and Nagai (1991) estimated the substorm onset to occur at 23 MLT \pm \sim 1.5 hours. After the onset, the precipitation area expands poleward. In addition, the area expands eastward with the drift of electrons with energy from 50 to 300 keV (Berkey et al., 1974).

The atmospheric effects of the strong ionisation has become subject for many recent studies. Codrescu et al. (1997) reported on EEP causing a significant increase in odd nitrogen ($NO_x = N + NO + NO_2$) and odd hydrogen ($HO_x = OH + HO_2$) at heights from 50-90 km. The species can catalytic destroy ozone and thus, alter the radiation balance in the middle atmosphere e.g.(Andersson et al., 2014) However, there are still big uncertainties on the detailed impacts of the precipitation (Mironova et al., 2015).

In order to estimate the global importance of EEP effects, we need more knowledge of the global spatial and temporal distribution of precipitating electrons, continuously (Turunen et al., 2009).Beharrel et al. (2015) found a way to model the ionisation at altitude of 80-90 km based on data from a global network of magnetometers (SuperMAG¹). This model is fixed at magnetic midnight and does not consider how the ionisation develops through the night. As SuperMAG is a global network, there is a potential mismatch between substorm intensity and locally estimated EEP.

¹<http://supermag.jhuapl.edu/>

The subject of this study is to examine how the atmosphere responds locally to the EEP. The amount of ionisation is a good indicator for estimating HO_x and NO_x production. Events lasting for many days are especially interesting, since most of the existing literature consists of case studies. How the ionisation develops through periodic events is a key question. Furthermore, the sensitivity of CNA with regards to intensity, will also be studied. Therefore, a deeper examination of the nature and the occurrence rate of intense substorms, is of big interest. In contrast to earlier studies, where global indices have been utilized, this study is based on local effects over longer periods.

Chapter 3

Data and instruments

In order to study the local ionospheric development, riometers are used in combination with magnetometers. The riometers measure the cosmic noise absorption (CNA), which is caused by ionization in the D layer. In this way, the evolution of electron density in that layer can be monitored. Furthermore, the IL index is used to examine the disturbances in the magnetic field, especially due to auroral electrojets. The IL index is constructed from magnetometers in the IMAGE network. The subject for this study is the local ionospheric effects during the substorm phases. Therefore, the reduced Lapland version of instruments is used, as seen in figure 3.1.

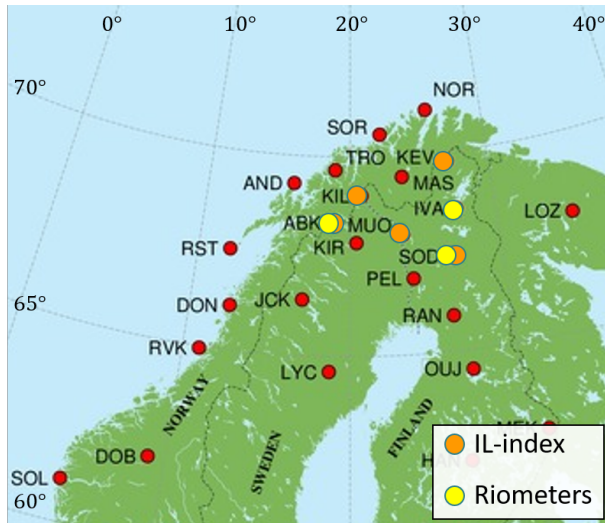


Figure 3.1: The map shows the stations used for the study. They are marked with orange and yellow. The red dots are magnetometers in the IMAGE network¹, not used in this study.

Code	Name	Geogr. lat (°)	Geogr. lon (°)	MLT - UT (hours)
ABK	Abisko	68.4	18.1	2.5
IVA	Ivalo	68.6	27.3	2.9
KEV	Kevo	69.8	27.0	3.0
KIL	Kilpisjärvi	69.1	20.8	2.6
MUO	Muonio	68.0	23.5	2.7
SOD	Sodankylä	67.4	26.6	2.8
TRO	Tromsø	69.7	18.9	2.5

Table 3.1: The table shows the names of the stations and their geographical coordinates. The time difference between magnetic local time (MLT) and Universal time (UT) is given in the last column. There is a time difference of 31 minutes between the easternmost and westernmost stations.

3.1 Cosmic noise absorption and riometers

The cosmic noise absorption (CNA) data are obtained from the three riometer stations at Abisko, Ivalo and Sodankylä (see table 3.1 and figure 3.1). Riometers are passive radio wave receivers that measure the amount of radiation from e.g. other galaxies or neutron stars. The received power depends, amongst other, on the electron density N_e and collision rate ν_{en} between neutrals and electrons. The Lapland receivers are positioned below the statistical auroral oval location. Hence, the instruments are appropriate for studying the electron density due to EEP from substorms.

As cosmic radio waves pass through the ionosphere, they are subject for refraction, dispersion and absorption. The refractive index μ , in an ionised medium with a background magnetic field, is given by the Appleton-Hartree equation (Appleton, 1932). A wave frequency $\omega < 30$ MHz, results in $\mu \ll 1$ above the D region (60-90 km). This means that the direction of the rays of cosmic radiation, changes when they collide with electrons. But $\omega \approx 30$ MHz results in $\mu \simeq 1$ such that the direction of propagating is not altered. Hence, they reach down to the D region where nondeviating absorption is more important (Zawdie et al., 2017).

The amplitude of a propagating radio wave decays exponentially as $e^{-\kappa x}$ where x is distance and κ is the absorption coefficient.

$$\kappa = \frac{e^2}{2\epsilon_0 mc} \cdot \frac{N_e \nu_{en}}{\nu_{en}^2 + (\omega \pm |\omega_{B_{||}}|)^2} \quad (3.1)$$

The first factors are constants where e is the electron charge, ϵ_0 is the vacuum permittivity, m is the electron mass and c is the speed of light. ν_{en} is the electron-neutral collision frequency. The gyrofrequency $\omega_{B_{||}}$ of the electrons, is calculated for the direction of propagation with respect to the magnetic field. Both ν_{en} and $\omega_{B_{||}}$ vary with altitude. ω is the frequency of the radio wave. A derivation can be found in e.g. McKay (2018). The absorption is caused by the electromagnetic waves accelerating the electrons. The electrons collide with neutrals resulting in a transfer of momentum. This takes place primarily in the

¹Map obtained from <https://space.fmi.fi/image/www/index.php?page=mapsh>

D region where ν_{en} is sufficiently high (Kero et al., 2014). During substorms with EEP, the electron density is increased in the nighttime D region. Consequently, cosmic noise is absorbed and the received power at ground level is decreased.

Finally, all this means that the CNA can be calculated by comparing the received signal with the quiet time without precipitation. By taking the ratio of the quiet-time power P_q and the received power P , the absorption of cosmic radiation can be expressed on a decibel scale as

$$A_{dB} = 10 \times \log_{10} \left(\frac{P_q}{P} \right) \quad (3.2)$$

where P_q is estimated from the corresponding medians of the last 10 days. If P_q can not be determined in this way, the closest P_q is used instead. From equation (3.2) one sees that the absorption A_{dB} increases whenever received power decreases. The absorption values are provided as 1-minute median values which typically range from 0 to 3 dB, but can also get as high as 6 dB. For this study, three riometer stations are used. To get the best match with the IL index, the upper envelope curve of the CNA data is calculated. The CNA for an examples substorm is shown in figure 3.2. The data can, however, look much more complex than this. In later figures, only the black upper envelope curve will be shown.

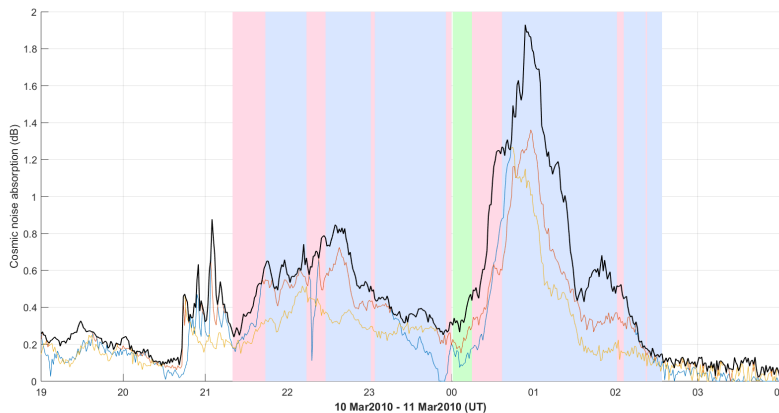


Figure 3.2: The figure shows the absorption during a -400 nT substorm. The blue, red and yellow lines represent the absorption A_{dB} at the stations of Abisko, Ivalo and Sodankylä, respectively. The thick black line is the upper envelope curve. The green, red and blue shadings represent the growth, expansion and recovery phase, respectively.

3.2 IL index

The Lapland version of the IL index is constructed from magnetometer data at Kevo, Kilpisjärvi, Muonio, Sodankylä and Abisko (see table 3.1 and figure 3.1). The location

of these stations make them especially favorable for examining the auroral electrojet, described in previous chapter. They are nearly co-located with the riometer stations and will therefore give the best possible match with the EEP. Since the substorm electrojet current is westward, the induced magnetic field causes a negative deflection in the north-south component of the Earth's magnetic field. The magnitude of the deflection is on order of hundreds of nanoteslas. The station closest to the current measures the largest magnitude. When all baselined data are plotted together, the lowest envelope curve the IL index (Kallio et al., 2000).

The baseline method in this study is an automatic one by van de Kamp (2013). By determining magnetically quiet days, they obtain a quiet curve (baseline) to be subtracted from the data of interest. In this way, the deviation due to magnetic disturbances are determined. In order to calculate the baseline, diurnal, lunar, seasonal and long-term variations amongst other factors have been considered. This is done for each station, separately. The lower envelope curve makes the IL index and is determined thereafter (Kallio et al., 2000). The magnetometers data are averaged over one minute.

The identification of substorm phases was done automatically using the method by Juusola et al. (2011). The criteria are:

1. Growth phase: from the IMF B_z turns negative and until the expansion onset.
2. Expansion onset: $IL < -50$ nT and $\frac{dIL}{dt} < -4$ nTmin⁻¹
3. Expansion phase: From expansion onset until recovery onset
4. From the minimum in IL index and until $IL > -50$ nT or a new expansion onset.

Compared to a manual identification by a trained eye, this identification results in rather too many phases instead of too few. In this way, one makes sure that no potential substorm signatures are missed. One can instead combine phase pairs if that should be needed.

3.3 Categories of substorms and periodic events

The IL index determines the phases and is therefore used to categorize the data from 2008 to 2013. The substorms were divided into -400, -600 and -800 nT substorms, each of them with an error range of ± 100 nT. Each day was then inspected from midnight to midnight as seen in figure 3.3 with respect to the minimum in the IL index. If the index, for instance, dropped down to values between -700 and -900 nT in the morning, this day was categorized as a 800 day. But if it also dropped down to -400 nT in the evening (figure 3.3b), it was also included in the 400 days since the two bays belong to two different substorms. This way identified from two to more than hundred days of interest per year. There were 582 days with IL index reaching -400 nT, 264 days with the IL index reaching -600 nT and 105 days with the IL index reaching -800 nT, which adds up to 951 days of interest in total. They were all evaluated manually afterwards and categorised according the minimum of the IL index.

However, if a bay had an index value of roughly -600 nT for a long time and dropped just below -700 nT for only 2 minutes, it would manually be categorized as a 600 day.

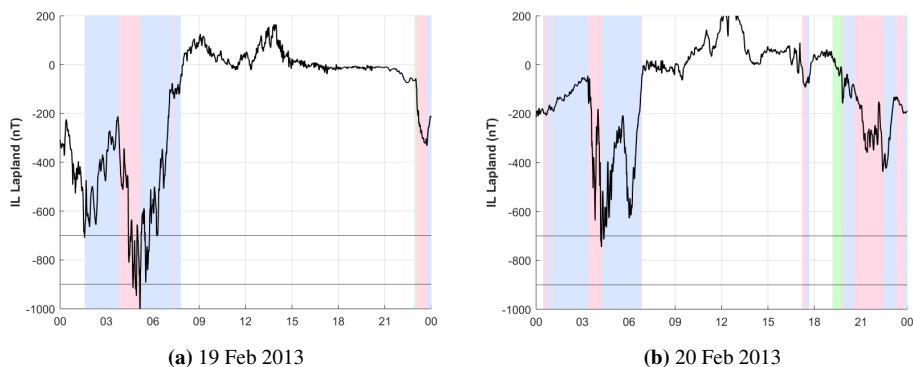


Figure 3.3: The figures show two consecutive days before they were separated into event nights.

This behaviour can be seen in the first bay in figure 3.3a. The first bay was categorised as a 600 bay. The second bay, was categorised as a 1000 bay, which is not an existing class in the categorisation and thus excluded from the data set. However, these two days were also part of a series of 7 nights, with substorm activity in a row. The entire chain of substorms was included in the multi-night category described below. So, the criteria were used as guidelines rather than actually rules to allow for discretion. Otherwise, good data would have been lost in a lack of a sophisticated enough algorithm. On the other hand, this manual filtering can be considered less consistent.

Finally, the days were combined in pairs, such that they together make one event night. An event night can either be a single night event or it can be one night constituting one multi-night event. During an event night there can be one or many substorms. Nevertheless, the event nights were subject for further manual evaluation. If there were two or more event nights in a row with substorms of similar intensity (e.g. -600 ± 100 nT), they were combined into multi-night event. Otherwise, only the first event night was used. The whole procedure gave a total of 120 events, consisting of 245 nights. By further analysis, it was found natural to divide the events into three categories, each with three different intensities as seen in figure 3.4 and table 3.2 and 3.3. Moreover, it was required that there was a quiet time of at least two days before the first event night for all the event types. In the quiet period, the IL index would not drop below -100 nT.

The definition by Sandhu et al. (2018) is used to distinguish isolated from compound substorms. Isolated substorms consists of one growth phase, one expansion phase and one recovery phase. If the first recovery phase is directly followed by a new phase pair, the substorm is defined as a compound substorm instead. A phase pair consists of one expansion and one recovery phase.

When evaluating the events, it was found that in practice an event night consists of one isolated substorm or one compound substorm, as seen in figure 3.6. The first night in figure 3.7 has three growth phases, which by definition means three substorms. Had that night been evaluated as a single night event, the phase pairs belonging to the first and latter substorms, would have been ignored. This can not be done for the last night in figure 3.8. That night would have been one of the very few single night events with more than

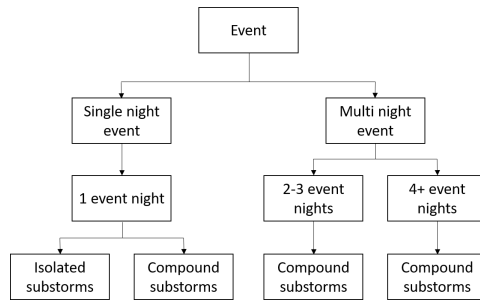


Figure 3.4: The figure shows a schematic representation of the event types. All of them are also separated into -400, -600 or -800 nT event nights.

	Single night: Isolated	Single night: Compound	Multi-nights: 2-3 nights	Multi-nights: 4+ nights	Total
-400 nT	15	16	12	8	51
-600 nT	2	25	5	7	39
-800 nT	2	19	7	2	30
Total	19	60	24	17	120

Table 3.2: The table shows the number of events for each type.

one substorm. Event nights similar to the second night (same figure), would have been evaluated as one long substorm. The single night substorms are in general simpler than those in the figures. For the multi-night events, discretion was not used. Instead, each night was evaluated from the first expansion phase to the last recovery phase. Furthermore, it is very uncommon for those events to have nights with isolated substorm. Consequently, this means that each night was analysed as one long compound substorm.

There are three types of events as described above. All of them are separated into three ranges of intensities. The single night events are further separated into two: isolated and compound substorms.

An example of an isolated substorms is illustrated in figure 3.5. They consists of one growth phase, one expansion phase and one recovery phase. It is uncommon that they

	Single night: Isolated	Single night: Compound	Multi-nights: 2-3 nights	Multi-nights: 4+ nights	Total
-400 nT	15	16	28	52	111
-600 nT	2	25	12	48	87
-800 nT	2	19	16	10	47
Total	19	60	56	110	245

Table 3.3: The table shows the number of event nights for each type of event.

occur two or more nights in a row. In that case they tend to develop into compound substorms instead.

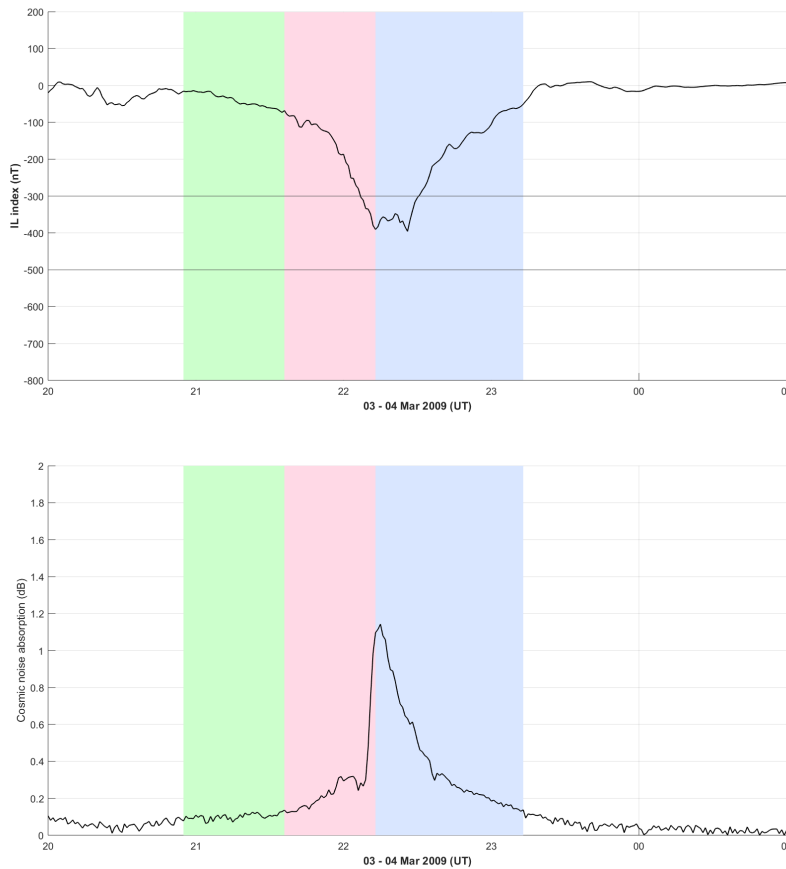


Figure 3.5: The figures shows an isolated -400 nT substorm during a single night. The top panel shows the IL index whereas the bottom panel shows the CNA.

An example of a compound substorm is illustrated by figure 3.6. They consist of one growth phase and two or more phase pairs. They can occur as single night event or as a multi-night event (2 nights or more). The activity during multi-night events consist, practically, only of compound substorms.

An example of a 2 night event is illustrated by figure 3.7. The category consists of two or three nights with compound substorms of the same intensity (± 100 nT). A perfect event will have a long quiet period followed by an event similar to the one in figure 3.7. During the second night, there is one small dip that drops below the lower threshold. The substorms is nonetheless, categorised as a -400 nT substorm. The first night has three growth phases, but a trained eye can easily see that there is only one substorm started by the second of the growth phases (at around 21:30 UT). The CNA is only calculated for

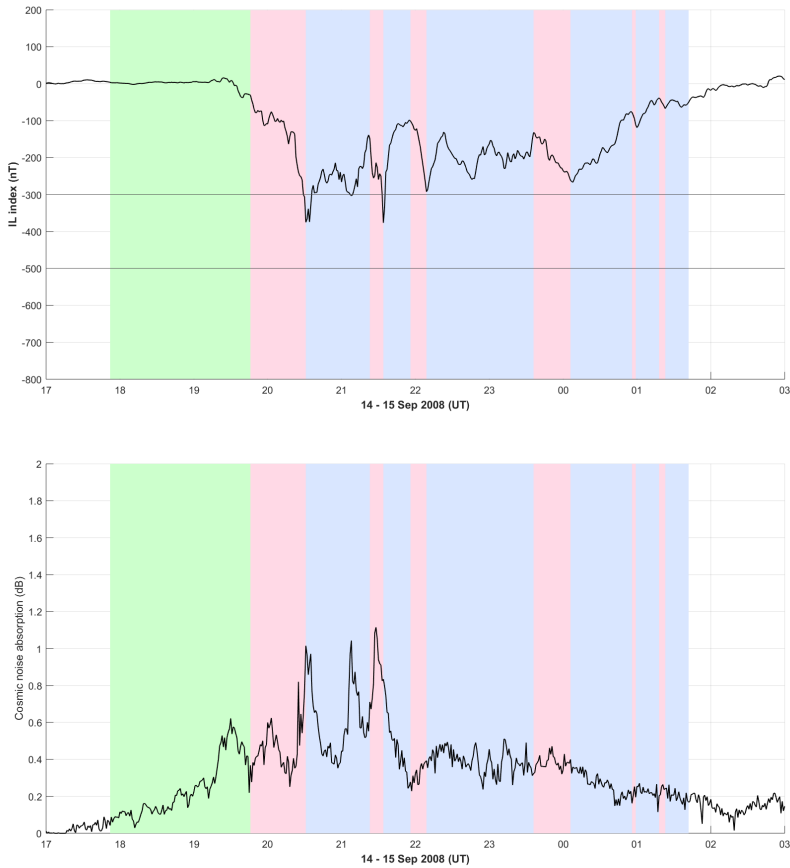


Figure 3.6: The figures shows a compound -400 nT substorm during an single night. The top panel shows the IL index whereas the bottom panel shows the CNA.

when there is either an expansion phase or a recovery phase.

An example of the events lasting for 4 or more nights is illustrated in figure 3.8. They consist of at least four nights and up to 20 nights of compound substorms of similar strength. There are bigger margins than the ± 100 nT used earlier. Without this margin, it would not be possible to get a long series of nights with substorm activity. The decision of which deviations that were accepted, was done manually and was typically of the order of 150 nT.

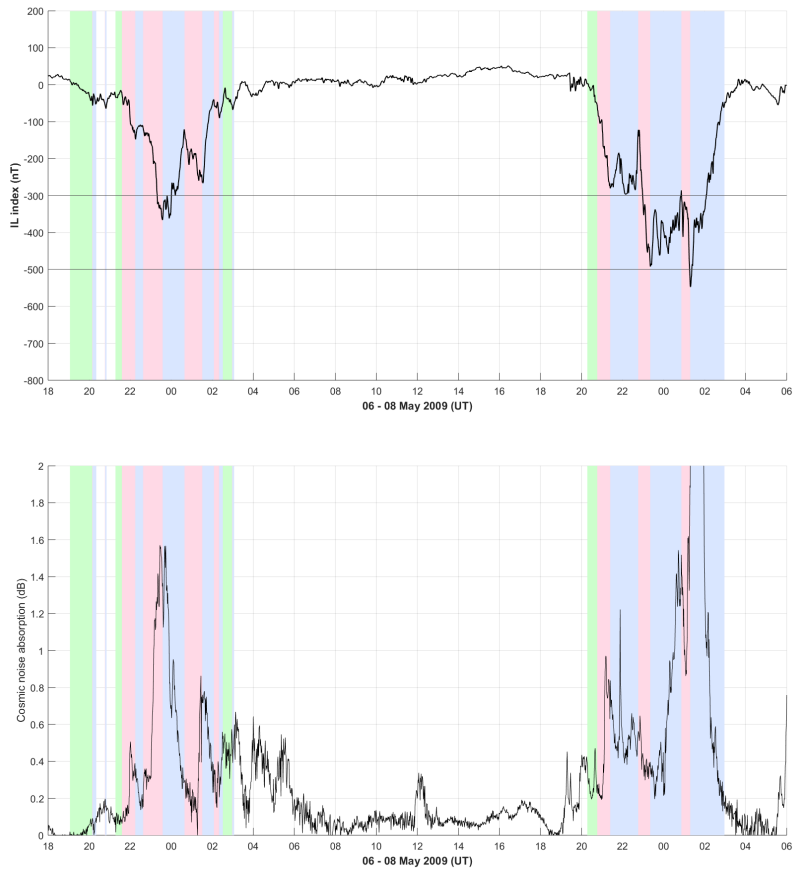


Figure 3.7: The figures shows a -400 nT 2 night event. The top panel shows the IL index whereas the bottom panel shows the CNA.

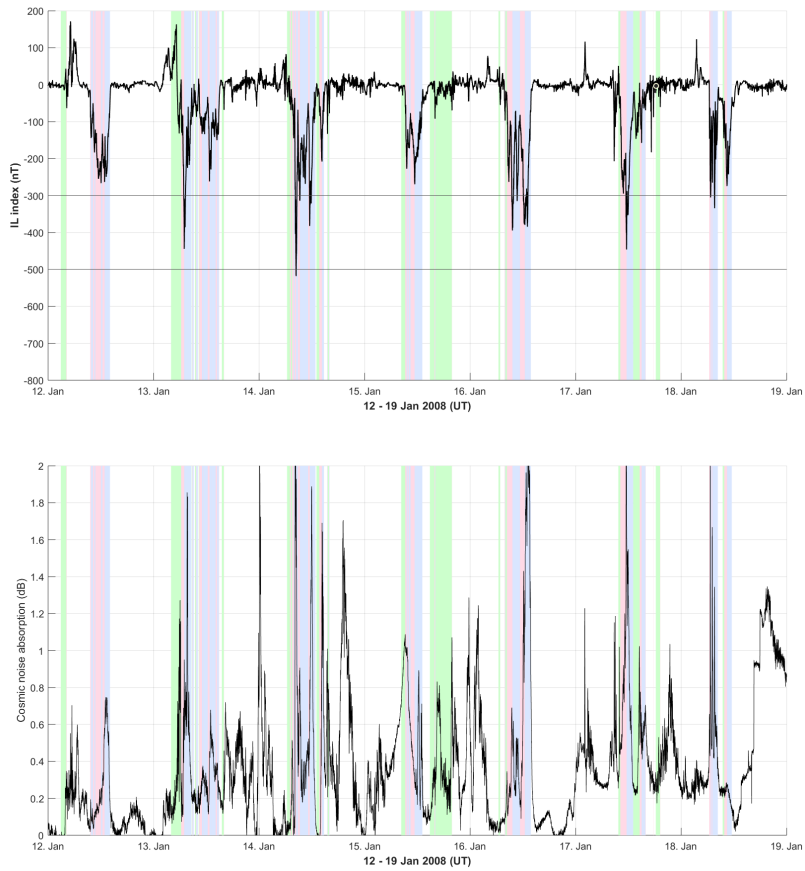


Figure 3.8: The figures shows an -400 nT 7-night event. The top panel shows the IL index whereas the bottom panel shows the CNA.

Experiment / Results

4.1 Correlation between substorm intensity and cosmic noise absorption

An evaluation of the correlation between intensity and CNA was considered as a natural starting point for further analysis. But this is not straightforward. As seen from figures 3.5-3.8, the duration of each night event can vary a lot. The duration is defined as the time from the first expansion phase to the last recovery phase. And the duration of each phase pair varies just as much. A way to standardize the data is therefore required to make it possible to compare different event types and substorms. Therefore, a total CNA refers to the integral of CNA from the start of the first expansion phase to the end of the last recovery phase. The CNA rate is the total absorption divided by the same duration. In the same way, the total absorption and absorption rate can also be calculated per phase pair i.e. from the start of the expansion phase to the end of the following recovery phase.

The total CNA and the CNA rate are plotted in figures 4.1 and 4.2, but should be read in light of the number of events and nights from table 3.2 and 3.3. There are for example 15 isolated -400 nT single night events. The median of the total CNA gives the first data point in the figure 4.1. This was done for all event types and for all intensities to obtain the 12 data points plotted in the figures. For the multi-night events, the total CNA and the CNA rate was averaged over all of the nights in the event.

By comparing the figures, it is evident that the isolated single night events are the most conspicuous ones. As mentioned in the previous chapter, the multi-night events basically do not include isolated substorms. Hence, figure 4.1 shows that for single night events, the total absorption is roughly 3 to 5 times greater for compound substorms than for isolated substorms. This makes sense since compound substorms must have a longer duration. Furthermore, one can see that the total absorption is smaller for compound single night events than for the multi-night events, even though the difference is much smaller than that to the isolated single night events. There tends to be a linear correlation between substorm intensity and total CNA. Note that there are only 2 and 3 isolated substorms of the intensity

of -600 and -800 nT, which makes the blue line at -600 or -800 nT less reliable. The data from the multi-night events are more reliable because of a greater number of nights per event. But they also have some variance in intensity.

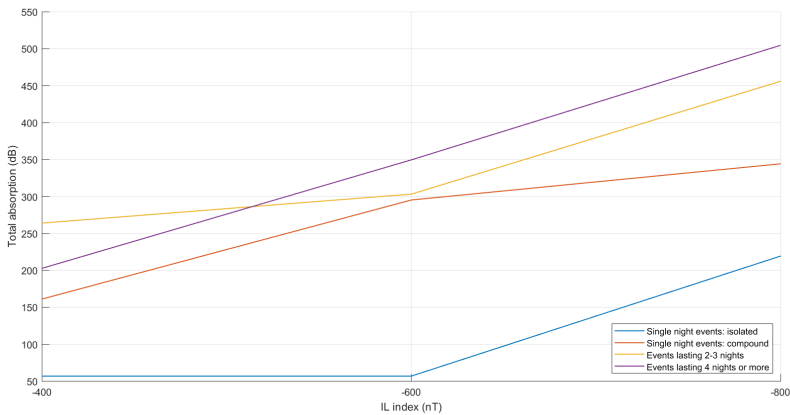


Figure 4.1: The figure shows the median of the CNA rate for all the event types and intensities.

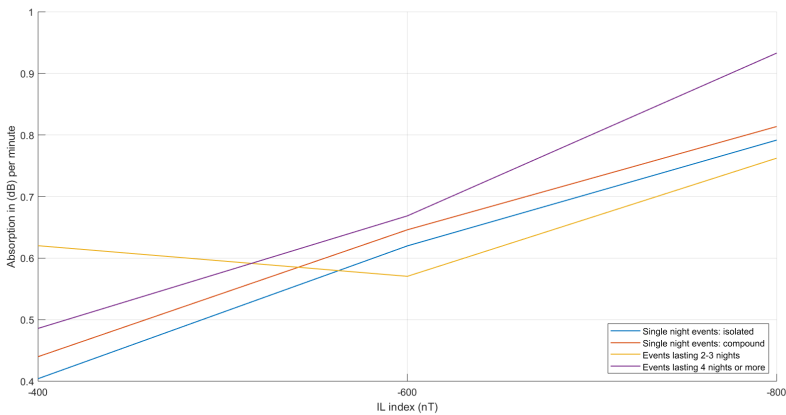


Figure 4.2: The figure shows the median of the total CNA for all the event types and intensities.

The correlations are interesting to study in light of the absorption rate. Despite the isolated substorms having a much smaller total CNA than the compound substorms, the absorption rate does not differ as much between the events. This implies that the compound events have a bigger total absorption mainly because of longer duration. For the -400 nT single night events, the difference in total CNA between the isolated and compound substorms is about 100 dB. The median duration is 110 and 360 minutes for the isolated and compound substorms, which can be multiplied with the difference of 0.05 dB/min in

absorption rate. Finally, one gets that 13 dB out of the 100 dB can be explained by an actual difference in absorption rate. Hence, the duration is the main factor for determining the amount of absorption. This is, only a rough estimate, but it shows that the compound substorms have a higher CNA rate than isolated substorms. This is examined further in chapter 4.4.

The multi-night events were calculated in a slightly different way than the single night events. They included some activity that a trained eye would not necessarily have called a substorm. This should in principle give a lower absorption rate. This can be seen in the -600 and -800 nT 2-3 night events in figure 4.2. The CNA rate of the -400 nT events deviates very much in comparison to all the other data plots. However, all the events lasting for 4 or more nights have a systematically higher absorption rate. This can either be because of internal or external factors. Either the CNA rate increases over time relatively to substorm intensity for long periodic events. Alternatively, the same mechanisms that allows for periodic events, also lead to higher rate of precipitation into the D layer. In that case, no evolution in CNA rate will be found. This is examined further in chapter 4.2 and 4.3.

4.2 Events lasting for 2 to 3 nights

In this section, the possibility for a systematic evolution of CNA between the nights is examined. Figure 4.3 gives the CNA rate for each night of the events. The coloured lines represent the different events whereas the black line gives the median of all events for the first, the second and the potentially the third night. For the -400 nT events, 10/12 have a higher CNA rate during the second night than during the first one. Only 1 event shows significantly lower absorption rate at night number two. For the third night, the CNA rate has decreased again for all of the events. There are only four events lasting for three nights in this intensity class. For the -600 nT events, there is a small decrease from the first to the second night and a greater decrease from the second to the third night. The variance for the -800 nT events is greater. Apart from two events, these events have a higher CNA rate during the second night as compared to the first one.

For comparison, the total CNA is also included and shown in figure 4.4. It mimics the CNA rate almost exactly. So despite absorption rate being less important when comparing different types of event, it seems to be heavily associated with the total absorption of its own event type.

4.3 Events lasting for 4 or more nights

The same method was also applied for the events lasting for 4 nights or more. The CNA rate is shown in figure 4.5. The black median curve of the -400 nT events shows an evident dip for the second night. This is despite that 5/8 events experience an increased CNA rate compared to the first night. After that, the median coincides better with the events which is calculated from. The result is an increase in a median CNA rate for each night until the night number 4. From then on, the median curve decreases. Note, however, that there are only 4 events lasting for more than 5 nights. The evolution is similar for the -600 nT

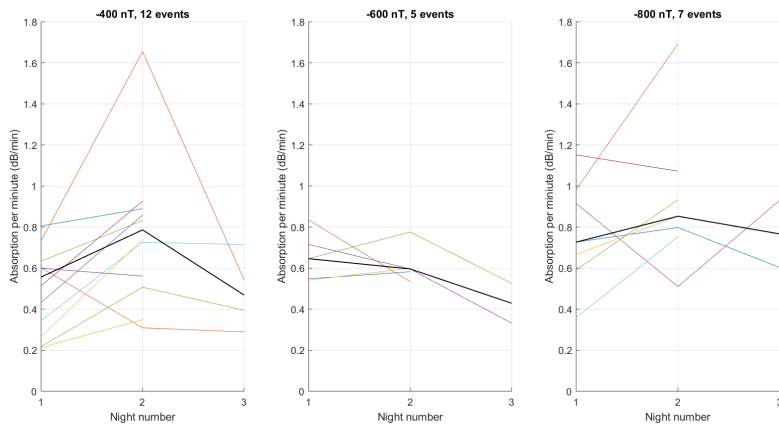


Figure 4.3: The figure shows the CNA rate for the events lasting for 2-3 nights for the three intensity classes. It shows how the CNA rate develops from night 1 to 2, and 3 if existed. Each coloured line represents a different event whereas the black line gives the median CNA rate value per night.

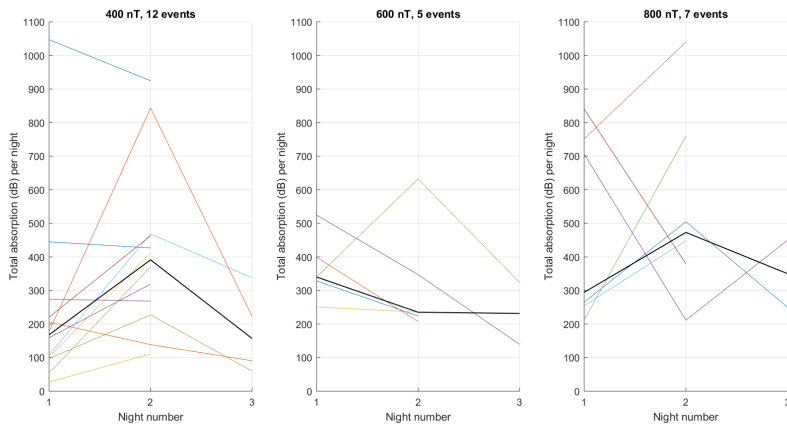


Figure 4.4: The figure shows the total CNA for the events lasting for 2-3 nights for the three intensity classes. It shows how the total CNA develops from night 1 to 2, and 3 if existed. Each coloured line represents a different event whereas the black line gives the median CNA rate value per night.

events, but here the CNA rate decreases already after the second night. There are too few events with the intensity of -800 nT to draw any conclusion.

As for the events lasting for 2-3 night, the total CNA is included in figure 4.6. The figure shows that the total CNA agrees very well with the CNA rate. This means that the duration of each event night must be very similar. Finally, it must be mentioned again that the substorm intensity can have a larger variance than the ± 100 nT. This means that the actual calculated values are less precise. But this error is systematic, and the trend of the

periodic events is the most important piece of information.

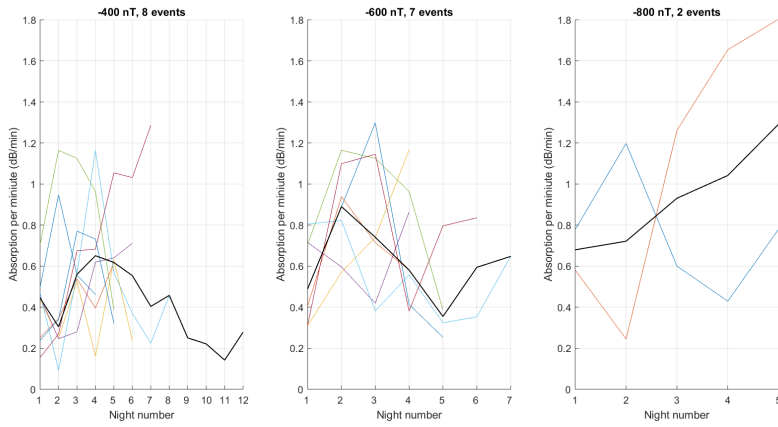


Figure 4.5: The figure shows the CNA rate for the events lasting for 4 nights or more for the three intensity classes. It shows how the CNA rate develops from one night to another. Each coloured line represents a different event whereas the black line gives the median of the first night, then second night and so on.

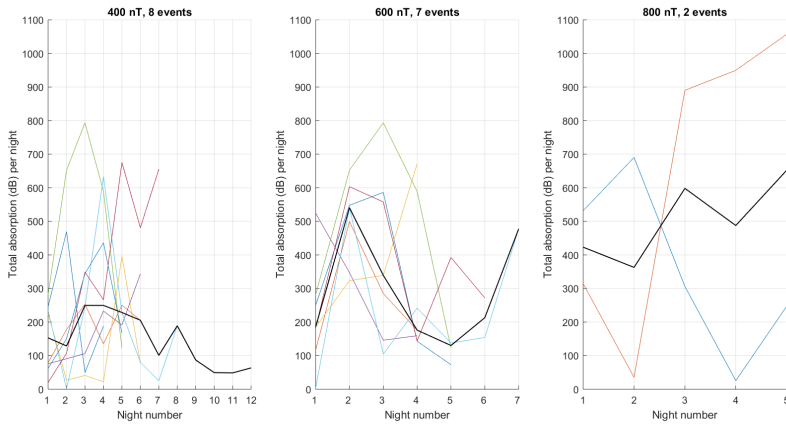


Figure 4.6: The figure shows the total CNA for the events lasting for 4 nights or more for the three intensity classes. It shows how the total CNA develops from one night to another. Each coloured line represents a different event whereas the black line gives the median of the first night, then second night and so on.

It is hard to draw any exact conclusion about the correlation between the nights. The substorm intensity and the number of events vary so much in the first place. One can see, however, that there seems to be a tendency for a peak in the CNA rate between the second and the fourth night. For future studies, a larger set of events would be required.

Nevertheless, the lack of isolated substorms is interesting. In practice, periodic events consists of compound substorm.

4.4 Compound substorms

The compound substorms of the single night events have more than 10 % higher CNA rate than the isolated substorms on average. In addition, they typically last about 200 minutes longer, excluding the growth phases. The nature of the compound substorms is therefore further examined in this chapter. This can also give a better understanding of the sensitivity of the CNA to the substorm intensity. To increase the size of the data set of compound substorms, all the nights of the multi-night events were split up into one big data set of single night events. As seen from table 3.3, this gives $245-19 = 226$ single night events instead of only 60.

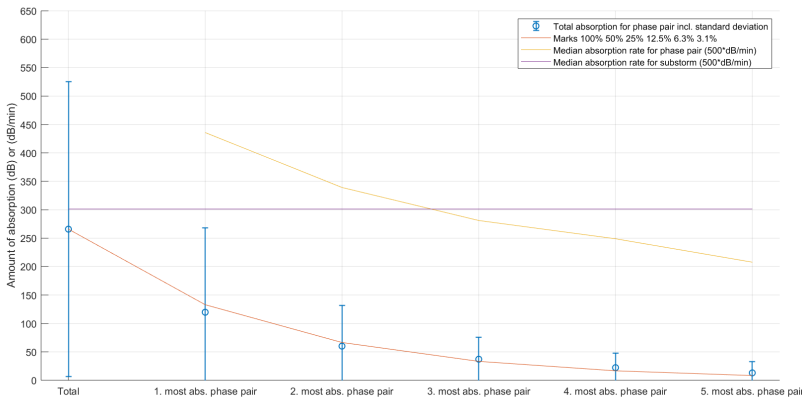


Figure 4.7: The vertical blue error bars represent the total CNA for each phase pair and the total CNA of the entire substorm (the first bar). They include 1 standard deviation. The red curve marks a halving of CNA rate. There are 226 evaluated nights. The purple line (at 300 dB) is the median CNA rate for all the nights. The yellow curve shows the median absorption rate for all of the phase pairs. Note that the yellow and purple curves have been multiplied by 500 to allow the curves to be plotted in the same figure.

First, the total CNA of each phase pair was saved for each event. Summing them up gave the total absorption for the entire substorm. Both the number of phase pairs and their duration vary a lot, which makes it meaningless to tell that e.g. a phase pair number three is the strongest. Instead, the sequences of phase pairs were sorted based on total CNA, so that phase pair one is the most absorbing one, phase pair two the second most absorbing one etc. This is plotted in figure 4.7 for all the 226 event nights, regardless of the phase pair intensity. There is a median total CNA of 263 dB, but there is an enormous deviation.

Surprisingly, the phase pairs tend to form a halving line. The red line in figure 4.7 marks 100 %, 50 %, 25 %, 12.5 %, 6.3 %, 3.1 % of the total absorption. Perhaps there is a doubling of CNA for each phase pair. If the initial CNA of a phase pair is 5 dB, it will

develop into a new phase pair with CNA of 10 dB before developing into 20 dB and so on. However, the timing of the phase pairs have not been taken into account. Hence, the phase pairs do not have to come in chronological order. This will be looked deeper into in the next chapter.

For comparison, the absorption ratios were also included in figure 4.7. The purple line gives the median absorption rate for all the compound substorms. The yellow line gives the median absorption rate for each of the phase pairs. Similarly, the absorption rates were calculated for the second to fifth most absorbing phase pair. The figure includes all the compound substorm for all three intensities. If the substorm categories are plotted separately, the shape of the curves are similar i.e. they follow the red line, but the actual values are different. As a result, one can see that the most and the second most absorbing phase pairs have an absorption rate above the median (purple line), whereas the other phase pairs have a rate below the median. The values of the yellow and purple absorption rates must be divided by 500 to obtain the correct absorption rates. It is the relative variations and not the numbers that are of most interest.

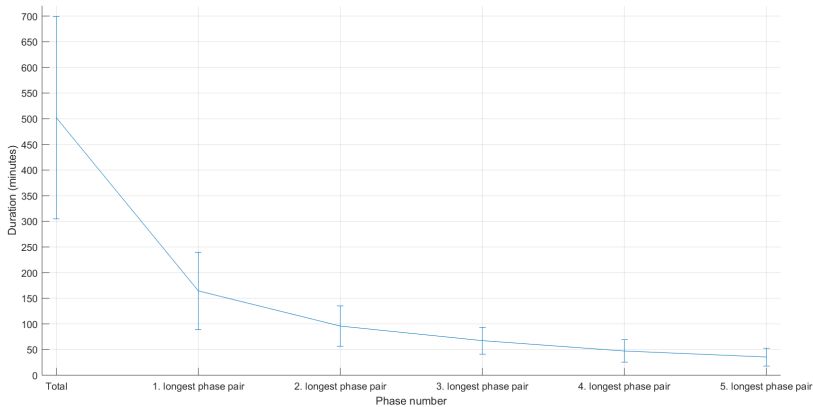


Figure 4.8: The figure shows the median duration and one standard deviation for the five longest phase pairs for all the 226 nights.

The same method was applied for evaluating the duration of each phase pair. The vertical lines in figure 4.8 give the median duration of the event nights and the median duration of the five longest phase pairs. The sum of the five phase pairs are 412 minutes, which means that on average are 90 minutes are not included in those five phase pairs. The total duration of 502 minutes is the time between the start of the first expansion phase and the end of the last recovery phase. On average, there are 6 phase pairs per nights, but the remaining phase pair lasts less than 35 minutes (see 5th longest phase pair). This means that about 60 minutes are not included in the phase pairs statistically. They are either identified as a growth phase (after the first) or not identified as any phases at all.

The actual absorption values are not taken into account here. Hence, the longest phase pair is not necessarily the most absorbing one. However, as described in chapter 4.1, the duration is the major driver of the total absorption when comparing the different event

types. The results from chapters 4.2 and 4.3 show that the absorption rate is more important when comparing events of the same type. That is not the case here. Therefore, it makes sense that there is a smaller variance in duration.

When the total CNA of the most absorbing phase pair (120 dB) in figure 4.7 is divided by the CNA rate (0.87 dB/min) of the most absorbing phase pair, one gets 138 minutes. This is 83 % of the 165 minutes for the longest phase pair in figure 4.8. The deviation is smaller for the other phase pairs. Hence, this is a good indication of the method giving valid results and that often the most absorbing phase pair is also the longest statistically.

To sum up, one sees that the total absorption, absorption rate and duration are strongly associated. Furthermore, the total absorption tends to follow the halving line for some reason. The mechanisms for this may be hidden in the order of the phase pairs. Does the most absorbing phase pair occur in the beginning, in the middle or in the end of the substorm? This will be investigated further in next chapter.

4.5 Timing of phase pairs

The focus of this section is to determine where in the compound substorm the most absorbing phase pairs occur. Do they occur in the beginning, middle or in the end? There are some major challenges in doing so. The standard deviations in figure 4.8 show a high variance in duration for the phase pairs. Consequently, it does not make sense to investigate how many minutes into the substorm the most absorbing phase pair occurs. It was found more informative not to include the duration and time.

The number of phase pairs has a normal distribution with a mean of 6 phase pairs. The number ranges from 2 to 13, but 66 % of the events consist of between 4 and 8 phase pairs. Note that the multi-night events are included in the data set. For comparison, the 60 compound single night events have a mean of 5 phase pairs. Nevertheless, the total absorption was evaluated against the number of phase pairs. This is shown in figure 4.9. The figure illustrates how often the most absorbing phase pair was the phase pair number one, two or three etc. A similar logic is followed for the second and the third most absorbing phase pair. The figure shows for instance that the most absorbing phase pair occurred as the first phase pair 24 times out of the total of 226 nights.

As mentioned before, the figures do not include the duration of the phase pairs. Therefore, the very short expansion phases lasting for less than 10 minutes can cause some bias. If there for instance, are two very short expansion phases prior to the most absorbing phase pair, the most absorbing phase pair will count as phase number three, even though a trained eye would have ignored those short-lived intensifications. This may make the distributions in figure 4.10 biased to the right. On the other hand, nights consisting of less than 3 phase pairs are not included. So bars one to three score relatively high, just because the shorter nights contributing less to bin 4 and higher. Anyway, it provides a way of comparing the -400, -600 and -800 nT events.

The events in the -400 nT category have the most absorbing phases pairs quite evenly distributed between the five first phase pairs before the number drop drastically from night five. The occurrence of the second most absorbing phase pair seems to peak around phase pair number 2 before gradually decreasing until phase pair number 7. The occurrence of the third most absorbing phase pair follows the same pattern, but peaks at phase pair 3.

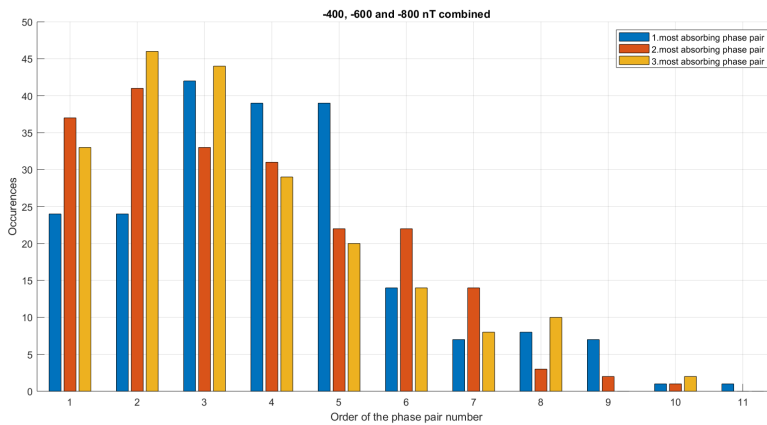


Figure 4.9: The figure shows how often the most, second most and third most absorbing phase pair occurs as the phase pair number 1-11 for the 226 evaluated nights.

This suggests that the first five phase pairs normally include the most absorbing phase pair, but that it is rather random which of them is the most absorbing one. From the fifth phase pair onwards there are either few phase pairs or they are in the category of the fourth most absorbing and, hence, not displayed in figure and of less interest. Based on the halving line in figure 4.7, these less absorbing phase pairs should only constitute about 13 % of the total absorption. In the end, it is worth noting that the first phase pair more seldom is the most absorbing phase pair for the -600 nT and -800 nT events than for the -400 nT events.

The most absorbing phase pairs look like a normal distribution for the -600 nT events and peaking at the fourth phase pair. The second most absorbing phase pairs do not have an evident peak while the third most absorbing phase pair has. But all three of them show a gradual decay in the occurrence rate towards the late phase pairs until about the eighth.

The events in the -800 nT category, on the other hand, do not have an evident form for the distribution. The most absorbing phase pairs are in general shifted towards later states of the substorm. One can argue that there may be a mild maximum around the third and fourth phase pair in case of most absorbing phase pair. Nevertheless, there are only a half the number of events as compared to the less intense events. The data set is smaller, but it is distributed over a greater number of phase pairs. Hence, the distribution becomes broader with a less evident peak.

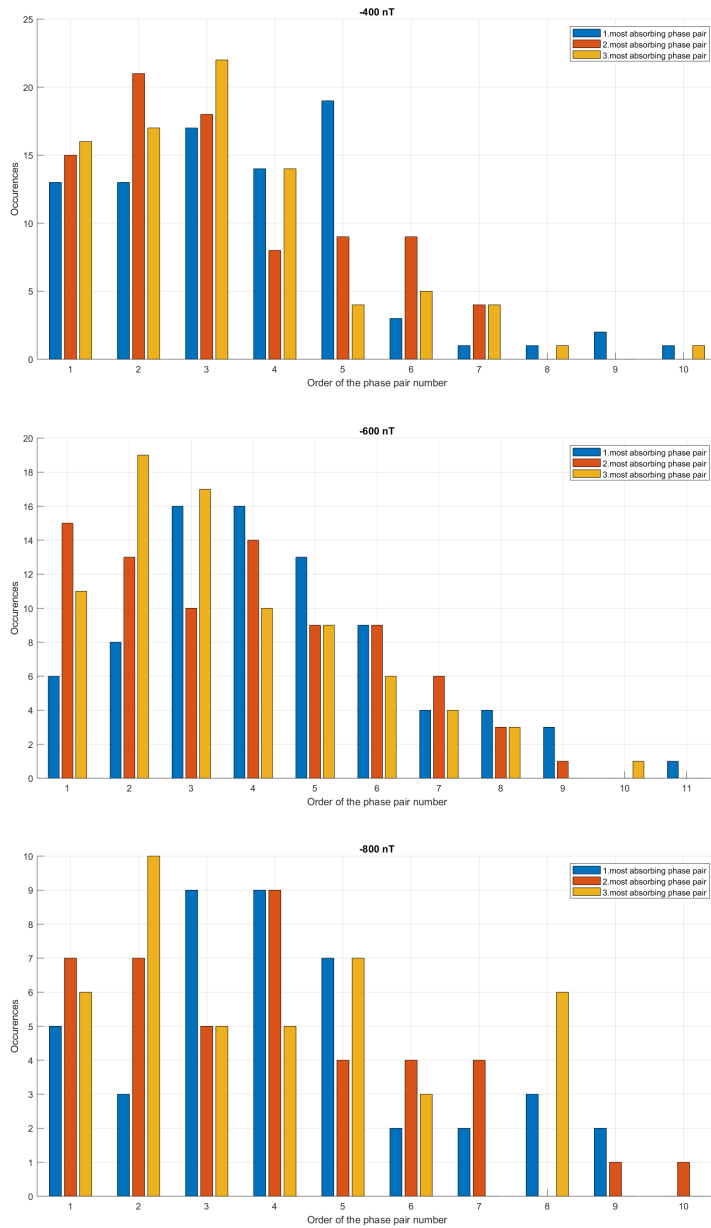


Figure 4.10: The figure shows the same as figure 4.9, but now the 226 event nights are separated into the intensity categories of -400, -600 and -800 nT, resulting in 96, 85 and 45 events, respectively.

Example event: 10-12th July 2013

The previous chapters have focused on giving an overall view. But many of the important features can drown in the statistics. Therefore, two events will be studied in more detailed in this chapter. They show some different characteristics that can explain the previous results better. While the statistics is the skeleton, the case studies are the meat.

In the period from 9-12th July 2013 there were three nights in a row with substorms. The substorms peaked at -600, -800 and -700 nT, respectively. The last substorm preceding this event took place the 6-7th July. Data from the EISCAT¹ very high frequency (VHF) radar in Tromsø is also available for this event. However, especially the first night's data was dominated by mesospheric echoes. Therefore, only the two last nights are discussed. The radar measures electron density at different altitudes. In contrast to the riometer, it is a point measure with a beam width of the order of a few degrees. During the experiment, it was pointed in a field aligned direction and probing the lower altitudes from 60 to 180 km. The radar site is marked by "TRO" at the map in figure 3.1.

In addition, solar wind data from the advanced composition explorer (ACE) satellite² is used. The data is time shifted with respect to the current bulk speed of the solar wind. Hence, the time axis of the data corresponds to when the solar wind arrives at the magnetopause of the Earth.

Ring current data from World Data Center for Geomagnetism, Kyoto³ was also used and plotted in figure 5.1. The disturbance storm time (Dst) index works in similar way as the IL index, but measures the ring current in the equatorial plane. The index is used for determining geomagnetic storms (Partamies et al., 2013).

5.1 An intense triple compound substorm

The substorm occurring the night 10-11th July 2013, shows a stepwise compound substorm (figure 5.2 and 5.3). The growth phase in the middle is ignored. The IL index reaches

¹Data obtained Nov 2019 from <https://eiscat.se/>

²Data obtained Nov. 2019 from <https://sohoftp.nascom.nasa.gov/sdb/ace/daily/>

³Data obtained Nov. 2019 from http://wdc.kugi.kyoto-u.ac.jp/dst_final/index.html

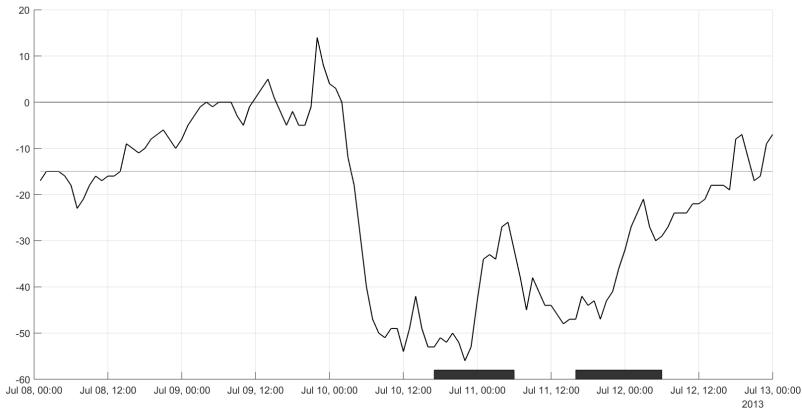


Figure 5.1: The figure shows Dst index (nT). The two black bars mark the periods of events being analysed.

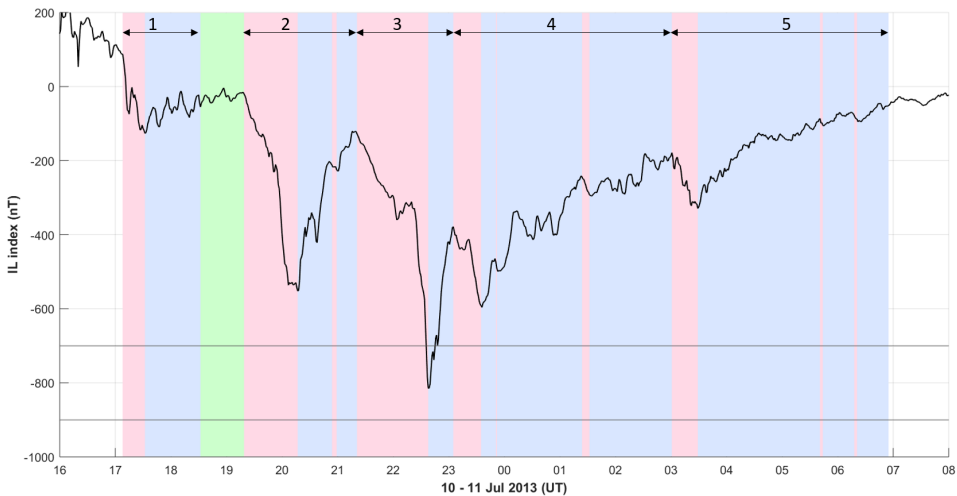


Figure 5.2: The figure shows the IL index. The horizontal lines marks the ± 100 nT for the -800 nT category. The numbered arrows at the top indicate the phase pairs.

a lower level for each expansion phase until it the minimum of -800 nT at 22:45 UT. According to Partamies et al. (2013), compound substorms are more common during the main phases of geomagnetic storms, which is the case here. Figure 5.1 shows that the Dst turns negative (main phase onset) already at 02:00 UT (preceding night) and stays low until the storm recovery onset at 22:00 UT. The storm recovery phase lasts until the evening next day.

The solar wind is often suggested as the main factor for controlling the energy transfer during substorm events. As seen in figure 5.5, the IMF B_z was negative practically the

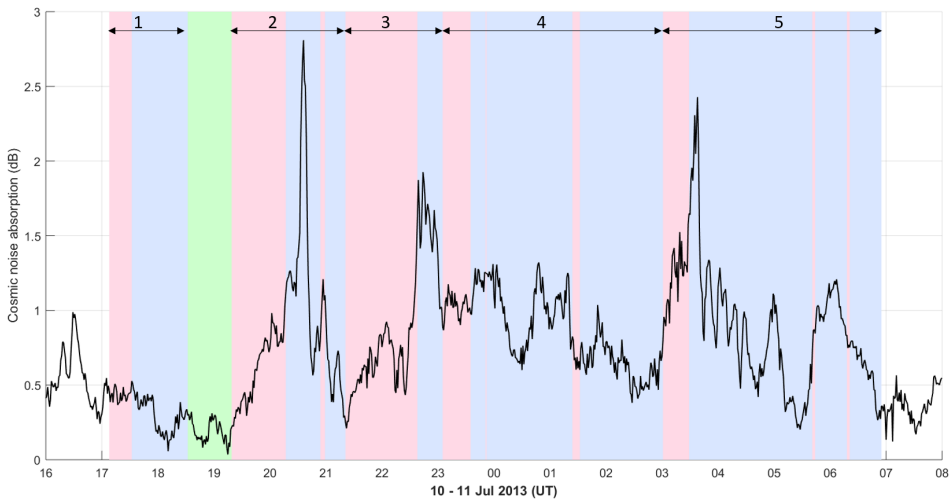


Figure 5.3: The figure shows the CNA. The numbered arrows at the top indicate the phase pairs.

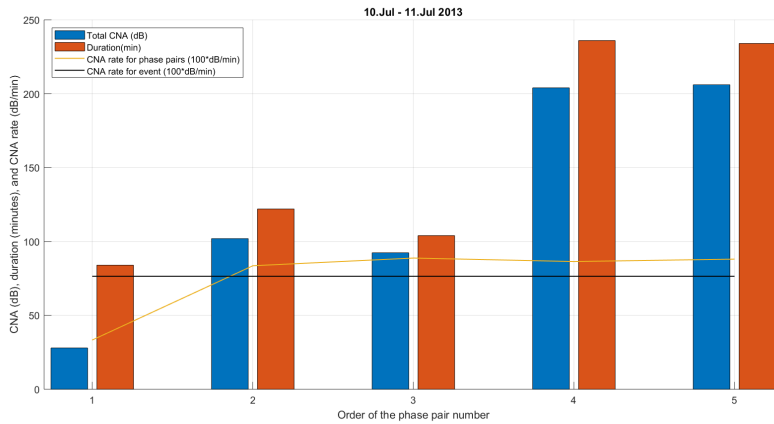


Figure 5.4: The bars show the total CNA and the duration for each phase pair. The yellow line shows the CNA rate per phase pair and the black line shows the CNA rate for the entire event. Note that the CNA rates have been multiplied by 100 to allow them to be plotted in the same figure.

entire night. The result is a high energy input to the magnetosphere, well above Akasofu's (1981) substorm threshold (10^{11} W). Actually, B_z was negative from 02:00 UT on the 10th July and the entire day of 11th July, with $\epsilon > 5 \times 10^{11}$ W prior to this substorm.

As for the CNA in figure 5.3, one should note that the data have elevated values (~ 0.5 dB) already prior to the substorm. To simplify the analysis, short-lived intensifications are combined to longer duration phase pairs to better assess the significant ionospheric changes. Therefore, the data for the 2nd-3rd phase pair, the 5-7th phase pair and the 8-

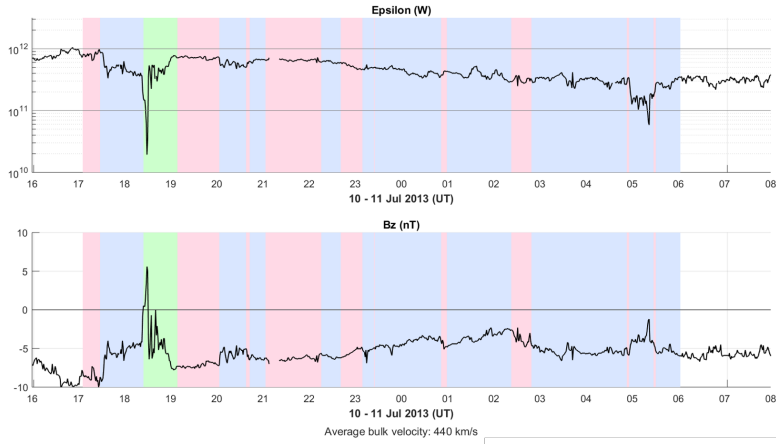


Figure 5.5: The top panel shows the energy input ϵ (W) and the bottom panel shows the IMF B_z measured by the ACE satellite. The times on the x-axis are shifted such that they show when the IMF reaches the magnetopause. The time shift is calculated from the solar wind bulk speed of 440 km/s.

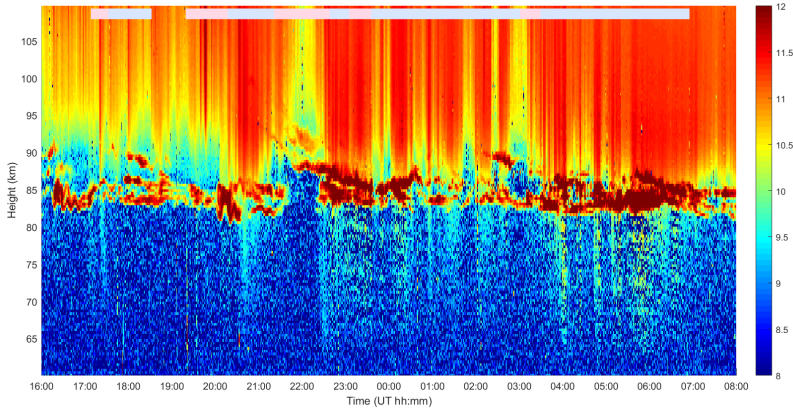


Figure 5.6: The figure shows the electron density (m^{-3}) measured by EISCAT VHF. The radar was pointing in the field aligned direction. The red and blue bars at the top mark the 5 phase pairs.

10th phase pair were combined, giving a total of five phase pairs as shown in figure 5.4 and at the top of figure 5.2 and 5.3. These combined phase pairs are hereafter, referred to as phase pairs 1 to 5. The CNA increases during the second phase pair. But the maximum occurs only in the recovery phase, not during the expansion phase. Thereupon follows a short-lived intensification prior to the phase pair of which the IL index reaches a minimum of -800 nT at about 22:30 UT (\sim 02 MLT). Again, the CNA peaks during the recovery phase, despite the energy input being high throughout the substorm. This can be caused

by a loading-unloading cycle. For the direct-driven model, the precipitation would have been more stable because of the stable solar wind driving.

It is very evident that the third phase pair experiences the lowest IL index. Nonetheless, this phase pair is not the most absorbing phase pair, only the second most absorbing one. Taken the IL index recovery into account, the later phase pairs show surprisingly high levels of CNA. The long duration of the phase pairs towards the end of the substorm indicates a more stable magnetosphere that does not cause new substorms. It may be caused by the continuous loading from the solar wind.

Electron density evolution measured by EISCAT is depicted in figure 5.6 with the five phase pairs marked at the top. At the altitude around 85 km, the electron density is very high. This is a layer of ice crystals condensed in the cold summer mesopause, called Polar Mesospheric Summer Echoes (PMSE) (Barabash, 2004), efficiently scattering the radar waves. There is an abrupt electron density decrease across the layer, indicating that the electron density may have been higher at lower altitudes without the additional echo. It is still possible to see an increased electron density all the way down to ~ 65 km at 22:45 UT and from 04:00-06:00 UT.

The electron density at 80 km peaks around 21:00 UT, corresponding to the highest peak in the riometer data. The electron density enhancement at 21 UT is a transient feature, while later on high electron density values are observed over a time period of several hours (until about 7 UT). As for the riometer data, the strongest precipitation is observed after the beginning of the recovery.

5.2 Two compound substorms

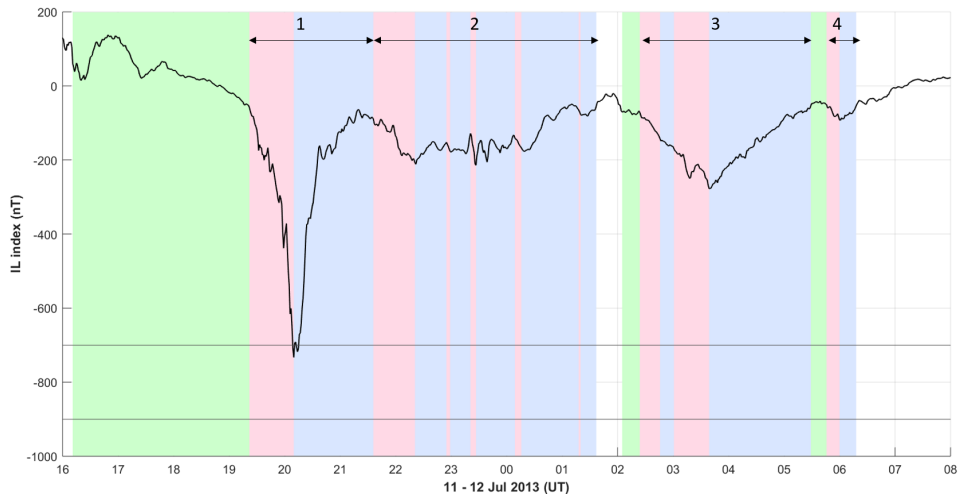


Figure 5.7: The figure shows the IL index. The horizontal lines marks the ± 100 nT for the -800 nT category. The numbered arrows at the top indicate the phase pairs.

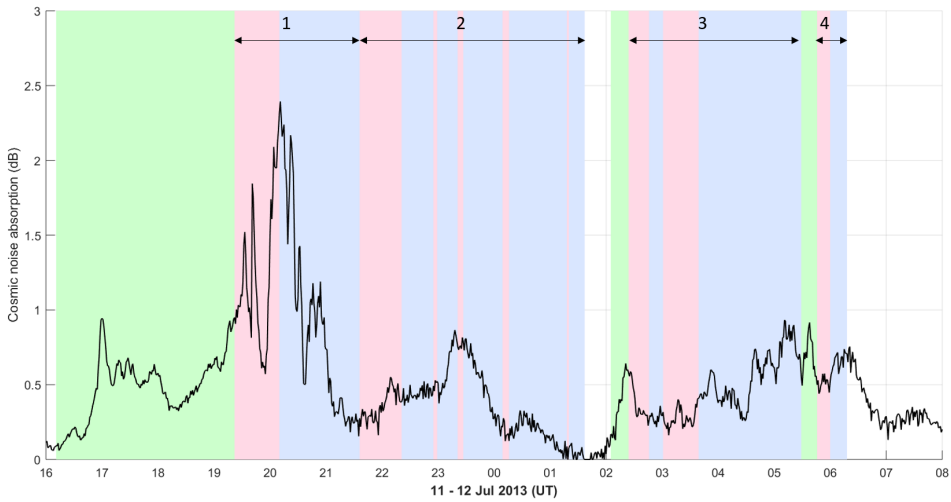


Figure 5.8: The figure shows the CNA. The numbered arrows at the top indicate the phase pairs.

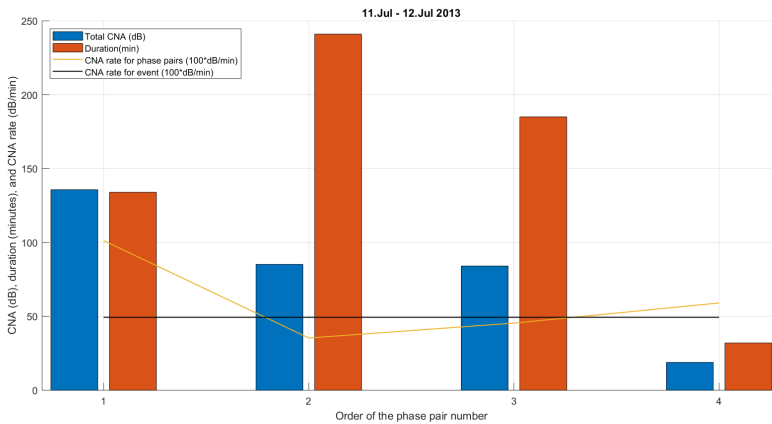


Figure 5.9: The bars show the total CNA and the duration for each phase pair. The yellow line shows the CNA rate per phase pair and the black line shows the CNA rate for the entire event. Note that the CNA rates have been multiplied by 100 to allow them to be plotted in the same figure.

The night of the 11-12th July 2013, in figure 5.7, show some different characteristics from the two former nights. First of all, the Dst index reveals a recovery of a geomagnetic storm, increasing -45 nT to -25 nT during the event. Secondly, during the first expansion onset at 19:22 UT, the IL index drops directly from -50 nT to -700 nT in 50 minutes. The following recovery phase lasts for 85 minutes and the IL index returns to -100 nT. This is typical behaviour for an isolated substorm, but in this case a phase pair follows directly thereupon. The following phase pairs until 02:24 UT could also be considered as one

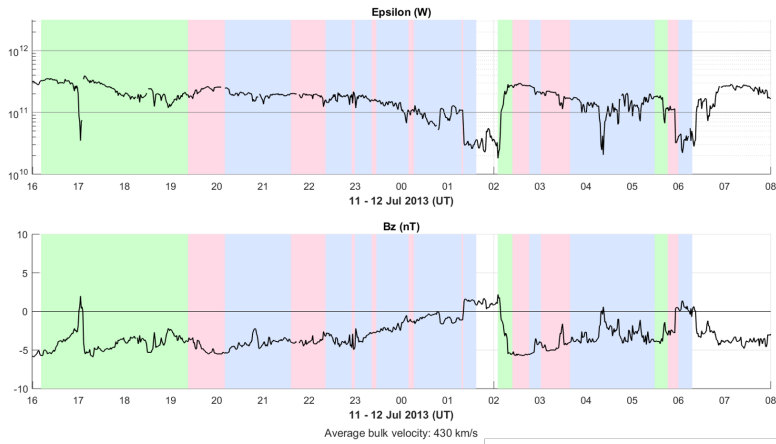


Figure 5.10: The top panel shows the energy input ϵ (W) and the bottom panel shows the IMF B_z measured by the ACE satellite. The times on the x-axis are shifted such that they show when the IMF reaches the magnetopause. The time shift is calculated from the solar wind bulk speed of 430 km/s.

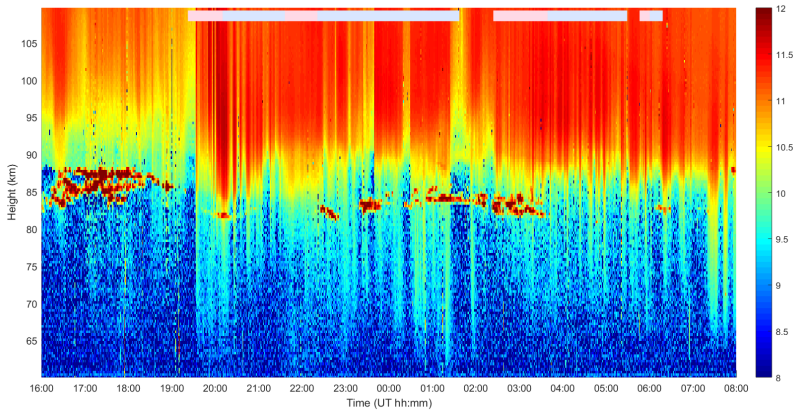


Figure 5.11: The figure shows the electron density (m^{-3}) measured by EISCAT VHF. The radar was pointing in the field aligned direction. The red and blue bars at the top mark the 4 phase pairs.

long substorm recovery. This agrees with the result of Partamies et al. (2013) in the sense that they found many substorm phase pairs of moderate strength during magnetic recovery phases. The IMF B_z is negative until the end of this substorm. However, the energy input described by the epsilon parameter (upper panel in figure (5.10) is lower than during the previous event, despite the similar bulk speed of the solar wind. Furthermore, towards the end of the substorm events, the energy input falls under Akasofus's (1981) threshold for substorm.

Short-lived intensifications were also combined to longer phase pairs in this event. The data for the 2-6th phase pairs and the 7-8th phase pairs were combined, giving a total of four phase pairs numbered as in figure 5.9 and at the top of figures 5.7 and 5.3. For this event, the first phase pair at 19:22 UT was the most absorbing one. In accordance with previous results, this phase pair also has the highest absorption rate. As suggested above, the most absorbing phase pair reaches high absorption due to the combination of a high CNA rate (1 dB/min) and long duration (134 minutes). In contrast to the previous night, the absorption rate decays soon after the maximum. The CNA peaks again at the beginning of the recovery phase. This suggests CNA being direct driven by the solar wind instead of loading-unloading cycle. There is also a small increase in the energy input from the solar wind. Despite the short-lived intensifications, one can see higher CNA values corresponding the negative bays in the IL index data.

This event could perhaps have been categorized as an isolated substorm. But it is clear that the 2nd-4th phase pairs show high CNA relative to the mild (> -300 nT) IL index. The total CNA the 11-12th July is still not comparable to the previous night. On the other hand, it is the two last phase pairs that are exceptionally high in absorption. The energy input is much lower this night.

The EISCAT data was less dominated by the mesospheric echoes this night, although some clear PMSE signatures are still seen at 16-19 and 22:30-03:30 UT. Figure 5.11 shows a smoother decrease in electron density across the D layer. There is a sudden electron increase at expansion onset of the first phase pair at 19:30 UT. It reaches down to ~ 67 km. The electron density is lower in the D layer during the next phase pair starting at 21:36 UT,

but taken into account the moderate values in both IL and CNA, the precipitation reaches surprisingly low altitudes. There are two significant intensifications of precipitation starting at 23:30 UT and 00:30 UT. The succeeding precipitation at 01:20 UT even reaches down 62 km, despite little change in the IL index. From 02:00 UT increases the electron density to $\sim 10^9 m^{-3}$ in the D layer during the short-lived intensifications. They can not be seen in the IL index, but are evident in both the EISCAT data and the riometer data. The precipitation does not reach below 70 km.

Discussion

6.1 Local effects

In this study, data from 3 riometers and 5 magnetometers have been analysed in the period 2008 to 2013. The instruments are located on a small geographically area, compared to the spatial scale of the substorms. This brings up both advantages and disadvantages. On one hand, it is easier to compare the data from the riometers and magnetometers precisely, simply because they are geographically close to each other. Occasionally, one finds big deviations from station to station, only amongst the riometer data, which shows the importance of local effects in the particle precipitation. Moreover, it is the the same part of the ionosphere that is studied throughout the night. This makes its possible to measure how ionospheric currents and EEP evolve over time from the first onset to the end of the recovery. The most disadvantageous aspect about this dataset is that a substorm is a global phenomenon. Had one monitored the magnetic midnight all the time could one, for instance, have seen multiple intense substorms. As the Earth rotates, the Lapland stations in this study would move from dusk to midnight and then into the dawn sector. Thus, it is hard to tell whether it is the precipitation directly from the substorm injection or only "side effects" of a substorm at magnetic midnight that is measured.

Kauristie et al. (1996) compared the global AL index with the EISCAT magnetometer Cross, which practically consists of the same magnetometer locations as those used for this study. For substorms with the intensity between -300 nT and -600 nT, the IL index measures higher values than the AL index at 20:00 to 02:00 UT and records at least 80 % of the activity in the sectors from 17:30 to 20:00 UT and from 02:00 to 04:00 UT (Kallio et al., 2000). The agreement with the AL index in the sectors before and after was not calculated.

The diurnal CNA typically peaks just before magnetic midnight and in the morning sector at 06:00-10:00 MLT (\sim 03:30-07:30 UT for Lapland) (Hunsucker and Hargreaves, 2002). This is indirectly related to the substorm processes in the midnight sector. Besides that there is a lack of a detailed statistically distribution of geographical area of electrons with energies high enough to penetrate down to the D layer. As described in chapter 2.4,

Beharrel et al. (2015) made a model for CNA in the midnight sector. Wing et al. (2013) made a precipitation model, but used an upper limit of 50 keV, thus only barely reaching down to the D layer.

The events that have been studied here had an average duration of 500 ± 200 minutes as seen in figure 4.8. The event on the 10-11th July was even longer with a duration of 840 minutes. The second to fourth phase pairs typically occur within the time period when the IL index measures lower values than the AL index, and therefore more precise. The first and most of the fifth phase pair lay within the time period that records at least 80 % of the AL index. This event night had much longer duration than most of the other events. Hence, it is safe to assume that the IL index agrees very well with the global index values, despite that these events have much longer duration than typical substorms found in literature, as reviewed in chapter 2

The precision of the IL index, with respect to the global processes means that the IL index can be relatively reliably used without considering the MLT in all magnetic local times sectors from late evening until early morning i.e. in the sectors where substorm activity can be recorded. Hence, it is safe to first categorise the CNA after IL index, and thereupon analyse how the CNA evolves in MLT. In this way, IL index and CNA can be used to make a global spatial and temporal distribution of EEP.

6.2 Phase pairs

As seen e.g. in figures 5.2 and 5.7, the number of short-lived intensifications lasting less than 10 minutes cause some bias to the analysis. They are simply too short to be real expansion phases, and do not contribute much to the overall absorption signatures. Consequently, what a trained eye would call one long phase phase, the algorithm may divide into two phase pairs. The statistical analysis of the duration and total absorption per phase pair becomes biased by the variance due to the increased number of phase pairs. One solution could be to set a minimum duration of 10 minutes as a criteria for the expansion phase. Then, for instance, the short-lived intensification at 23:05 UT in figure 5.2 would have been included, but the one at 01:35 UT would have been left out. In figure 5.7, only the short-lived intensifications in phase pair 2 would have been left out. In this way one could obtain more distinct separations between the phase pairs. That would have made the CNA analysis easier, especially in terms of the timing of the phase pairs in chapter 4.5.

If the same analysis had been done for the IL index as for CNA, the timing of the most intense phase pairs (IL) could have been compared with the timing of the most absorbing phase pairs (CNA). For the event the 11-12th July (figures 5.7 and 5.8), for example, phase pair 1 is both the most intense and the most absorbing phase pair. However, this is not the case for the event the 10-11th July (figures 5.2 and 5.3). Phase pair 3 is the most intense phase pair, but phase pair 4 and 5 are the most absorbing phase pairs, as seen in figure 5.4. This event agrees with the morning precipitation being relatively more intense.

Another point is that the most intense (with regards to IL) phase pair can be used a reference. The following phase pairs can be evaluated separately from those prior to this reference. The events in figures 5.2 and 5.7 suggest that it is more accurate to talk about a small number of long recovery phases rather than many shorter phase pairs. Expansion and recovery phases should perhaps have been analysed separately in the first place, since they

are controlled by different mechanisms. Interestingly, the absorption maximum is reached during the recovery phase rather than during the expansion phase, which, by definition, holds the deepest negative bay in IL index.

Finally, the categorisation has not always been consistent. During the visual inspection, some single night events have been shortened a little in order to leave out very small substorms. The event the 11-12th July in chapter 5.2 is a good example of this. In one way, it is the first substorm that is of most interest because it has the strongest IL index. In another way, the following substorm is also of interest as it is part of the same night and often has a high CNA. The second substorm was not left out because the event night was part of a multi-night event. It would have been left out if the event night was analysed a single night event. Moreover, the CNA is the main focus in this study. To leave out the smaller substorms for the single night events was therefore a bad choice. It creates a big inconsistency in the data set. And one can argue for the CNA in the early evening and late morning section being the most important. Being able to study those regions was one of the main arguments for using instruments limited to a small geographical area.

6.3 Substorm intensity and timing of phase pairs

The Lapland CNA was evaluated from 2008 to 2013 in the light of IL index for the same area. Demanding a quiet time for two days in the IL index prior to the first event night, shrank the data set considerably. This was done to reset a potential "memory" in the ionosphere. Nevertheless, the results showed that the isolated single night events were more common in the category of -400 nT events than among the more intense ones. On the other hand, compound single night events were significantly less common in the -400 nT category than among the more intense ones, as seen in table 3.3.

Furthermore, a linear correlation between substorm intensity and the CNA rate was shown in figure 4.1. The compound substorms have a higher CNA rate than the isolated substorms. This means that there are more electrons having high enough energy to reach down to the D layer. This energetic electron precipitation (EEP) corresponds to energies 10-200 keV (Seppälä et al., 2015; Turunen et al., 2009). As shown by figures 5.6 and 5.11 the EEP even reached down to the altitude of 65 km which corresponds to a particle energy of about 500 keV.

When categorising the events, the minimum level of the IL index was used. Thus, the minimum during the whole event determines the category, and an individual phase pair within the event may be less intense than the assigned category. This is more important for the less explosive compound substorm as described in chapter 2.2. If the CNA was linearly correlated with the IL index, the amount of CNA should have been reduced for the compound substorms. This means that IL index cannot explain the EEP alone. However, the data in the figure 4.1 is averaged over the whole substorm, which does not have to show a correlation between the IL index and CNA. An example of less correlation can be seen in the event on the 10-11th July in figure 5.4.

The statistical results of the timing of the phase pairs is shown in figure 4.10. One can not say for certain which MLT the later phase pairs actually correspond to. The occurrence of the most absorbing phase pairs peak as the phase pair numbers 3-5. The example events in figures 5.3, 5.8 and 3.6 to 3.8 show that those phase pairs can be expected from 00 UT

(~ 03 MLT) and later. For the substorms in the -400 nT category, the most absorbing phase pairs are evenly distributed amongst the first N phase pairs. They can therefore occur already at 20 UT (~ 23 MLT), which is estimated to be the average onset time for substorms (Nagai, 1991). However, figure 4.9 shows that it is more common that the most absorbing phase pairs, occur as one of the later phase pairs in the -800 nT substorms than during the -400 nT substorms. As discussed, this can also be because of short-lived intensifications are more common during strong events. Nevertheless, this implies that the CNA is important in the late night to morning sectors, and especially during the more intense events. The third phase pair ($\sim 05 - 08$ MLT) in figure 5.7 peaks at -300 nT. But the total CNA is 80 dB (figure 5.9), which is half of the total CNA for the entire -400 nT compound substorms. The IL index drops quickly during the expansion phase by definition. Hence, it spends longer time at lower levels during recovery phase, because dissipating the ionospheric currents takes longer than building up the strong currents due to particle injections. If one considers the time after the most intense phase pair (after phase pair 3 in figure 5.2) as one long recovery phase, it is understandable that the stronger substorm in the -800 nT category show higher CNA and that it happens during the later phase pairs.

Partamies et al. (2013) concluded that the recovery phases on average are twice as long as the expansion phases. In a comprehensive study by Oyama et al. (2017), it was found that the precipitation energy tended to increase with MLT in the morning sector, hence reaching lower altitudes, in accordance with Hunsucker and Hargreaves (2002). At the same time, the geomagnetic activity generally decreases with MLT. All this sums up to that the CNA cannot be explained by the intensity of the phase pairs alone. The linear correlation is only found in statistics when the CNA is averaged over the whole substorm duration. Oyama et al. (2017) concluded that their late morning increase in EEP was caused by pulsating aurora, which is typical in the morning sector and even after the recovery phase. Both figures 5.3 and 5.8 show the enhanced CNA in the morning sector very clearly.

6.4 Multi-night events

It is difficult to draw conclusion from the multi-night events. It was required that each night belonged to just one substorm intensity. Then it was examined whether there was any systematic absorption behaviour between each event night. Since these events range a time scale of days, the ± 100 nT becomes quite narrow categories. An extra margin was needed for the events lasting for more than 4 days. Therefore, it would have been better to evaluate the multi-night events in one group regardless of the IL index. That would have increased the number of events significantly. The less strict criteria would also have resulted in higher consistency as exceptions in the substorm intensity categorization would not have been needed. Figure 3.8 shows this very well.

The big variance in CNA from night to night can be explained better by external factors like geomagnetic storms. The events presented in chapter 5 occurred during storm main- and recovery phase, respectively. The IMF B_z was negative practically throughout both the event. The energy input was lower during the second night. Tanskanen (2002) found the substorm intensity to be mainly controlled by the energy input during the expansion

phase. They also found substorms less intense than -400 nT to be almost absent when $Dst < -40$ nT. This agrees well with both cases in chapter 5. Also, Sandhu et al. (2018) argued for compound substorms being associated with strong solar wind driving and energy input to the ring current. Both the IL and Dst indices were more disturbed during the first night than the second one. The Dst evolution was, however, not examined for the rest of the multi-night events, but only for the isolated single night events. All the isolated -800 nT substorms occurred during weak geomagnetic activity while none of the -600 , but 3 of the -400 nT substorms did so.

6.5 Compound substorms

Another important feature is the duration of the compound substorms. On average, only the longest phase pairs last for ~ 3 hours (growth phase excluded), which is only slightly longer than the textbook examples of isolated substorms (McPherron et al., 1973; Kullen and Karlsson, 2004). Instead, it is the number of phase pairs that make the substorms so long. Tanskanen (2002) reported, however, that substorms with continuously solar wind energy input lasted for 4 hours instead of 3h 13 min. As seen in figure 4.8, the average duration was 500 minutes (~ 8 hours) for the 226 event nights that were evaluated. 166 of these events were part of a multi-night event. Only 60 of the events were single night events by the original definition. It has been discussed above, that only those were evaluated as true compound substorm with only one growth phase. The 166 event nights could actually consist of many smaller substorms, which explains the very long duration.

That is the largest bias in the whole study: me. When I started working on the the data, I had an understanding of compound substorm being a special phenomena that differed very much from the isolated substorms. That is why the single night events were shortened. By ignoring the less intense substorms, it became easier to study the ionospheric effects of the compound substorms. As discussed earlier, it would have been a better choice to evaluate all the event nights in the same way as the multi-night events: use the first expansion phase and last recovery phase as start and end of the event. If there was a time gap between the phase pairs like at 02 UT in figure 5.8, the CNA during the gap should not have been ignored. In the same way, can there be a growth phase between phase pairs. They can be included and analysed in the same way as a gap. Growth phases prior to the first phase pair can be very long when defined by the IMF B_z turning negative. If the growth phases should be included, the duration of the phases should be considered first.

To sum up, 226 event nights, with precipitation going on for many hours, have been examined. Earlier studies have focused on isolated substorm, probably to avoid the human bias and the difficulty in the determination of the phases, phase pairs and more complex substorm types. They have in general a lower CNA rate than those lasting for many hours, as seen in figures 4.1 and 4.2. Consequently, the total CNA is much higher for the longer events. It is plausible to believe that the amount of CNA is indirectly controlled by the solar wind and therefore geomagnetic storms. This can cause the energy content in the ring current to increase as Sandhu et al. (2018) suggested. They argue for the particles being accelerated in the ring current region. Hence, they can penetrate deeper into the atmosphere. So is the ionosphere affected by this?

6.6 Atmospheric effects

In chapter 2.4, some of the atmospheric effects of EEP were outlined. EEP can be a contributing factor for the radiation budget. Seppälä et al. (2015) analyzed a five days long event ($-400 \text{ nT} < \text{AL} < -1000 \text{ nT}$), which is very similar to the multi-night events examined in this study. They concluded that such an event can destroy 5-50 % of the ozone at the height of 70-90 km, depending on season. The depletion recovered after a couple of days. Similar recovery was reported by Andersson et al. (2014).

A total of 245 event nights (table 3.3) from a period of 6 years analysed in this study. Before the quiet time was required, the data set consisted of 951 days of interest. On one hand, the number should have been smaller since two days of interest only makes one night of interest. On the other hand, days of interest often occur in a row. There were many substorms that were more intense than -800 nT , which were filtered out. If there were e.g. 1000 days of interest, a substorm, more intense than -400 nT , occurred every other day in the 6 year period. Both Seppälä et al. (2015) and Andersson et al. (2014) reported an ozone recovery time on the scale of days. Consequently, this very simple estimate shows that the ozone on average will have little time to recover between the EEP events. The occurrence rate of these events is so high, that the precipitation can possibly be a significant parameter for the atmospheric chemistry on regular basis.

However, the study by Seppälä et al. (2015) consisted of a 5 days long period. In this study, an evident correlation from day to day was hard to find for the multi-night events. It seems to be controlled mainly by external factors. Nevertheless, the simple estimate will not be correct as many of the nights with intense substorms come in a row, possibly during geomagnetic storms. Therefore, it would be interesting to look more into the correlation between CNA during geomagnetic storms.

Conclusion

The evolution of EEP in the ionosphere above Lapland was examined by using 3 riometers and 5 magnetometers in the period from 2008 to 2013. During this time span, 245 event nights were evaluated. 79 of them occurred as single night events, while the remaining 166 came in groups of at least 2 event nights in a row.

Most of earlier studies of CNA have focused on the magnetic midnight section. In this study, only a small part of the ionosphere was examined, but the events in this study had an average duration of about 8 ± 3 hours. During this time, the instrument stations move from magnetic evening to late morning region as the Earth rotates. In this way, the evolution in CNA can be studied with respect to processes that are typical for that MLT. At the same, the history for that night is included. This was also done for events consisting of multiple nights in a row. In those cases, substorms of similar intensity were required. The magnetometers were used to define the growth, expansion and recovery phases of the substorms. They were also used for separating the substorms into a -400, -600 or -800 nT category based on the minimum in the IL index. The CNA was analysed in light of those categories.

First of all, a linear correlation between intensity and CNA was found when averaging the CNA from start to the end of each event night. But when the single night events were analysed in detail, it was shown that the CNA is not only controlled by the substorm intensity. Both the cases in chapter 5 and literature suggest that the CNA in the morning section is relatively high. This does not mean that the phase pairs in the morning sector necessarily are the most absorbing ones. Figure 4.10 shows otherwise. The most absorbing phase pairs most often occur as phase pair number 3-5. It is only compared to the IL index that the CNA is especially high. Nonetheless, both figure 4.9 and 5.6 shows that there are exceptions.

Furthermore, it was shown in table 3.3 that the isolated substorms are uncommon in the intensity category of -600 and -800 nT substorms. This implies that the intense substorms are associated with a more unstable magnetosphere and stronger solar wind driving. Based on this, parts of this study focused on compound substorms. It had been a better choice to evaluate the night from the first sign of activity and to the end of activity. In the end,

the phases are nothing more than definitions based on the magnetic deflections measured on the ground. However, the CNA does not correlate directly with the IL index. It should therefore primarily be used for defining the maximum substorm intensity that night. From there, it is more informative to evaluate the CNA with respect to the MLT.

Moreover, the CNA seems to be controlled mainly by external factors like the solar wind driving and the ring current dynamics. There may be a potential correlation between the nights such that nights 2 to 4 have a higher CNA than the rest as seen in figures 4.3 - 4.6. This correlation can possibly be caused by the external factors. For future studies of CNA evolution during substorms, the Dst index and solar wind data should also be included - especially for studies of multi-night events.

Finally, The events in this study are comparable to events in earlier studies of ozone depletion due to EEP (Andersson et al., 2014; Seppälä et al., 2015). As seen in figure 5.6 and 5.11, -700 nT substorms can have EEP with energy high enough to penetrate deep into the D layer - even down to the altitudes of ~ 65 km. Hence, also the less intense substorms may have EEP with high enough energy to indirectly alter the amount of ozone in middle atmosphere. According to the earlier studies, most of the ozone recovered within a couple of days. But even with the condition of a quiet time prior to the event, 245 event nights were found in 6 years. This number is much higher without the quiet time. My guess is that a correct number is of the order of 1000, i.e. one event every other day on average. Despite many of the event nights occurring in a row, the number should be high enough that new intense substorms can occur before the ozone have had time to recover. This shows that the EEP is not only important for the chemistry on short time scales. The occurrence rate of these events is so high, that the precipitation can possibly be a significant parameter for the atmospheric chemistry on regular basis.

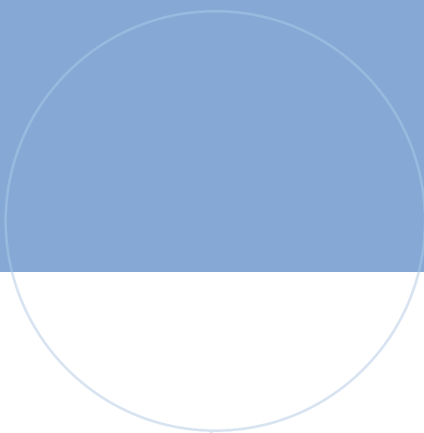
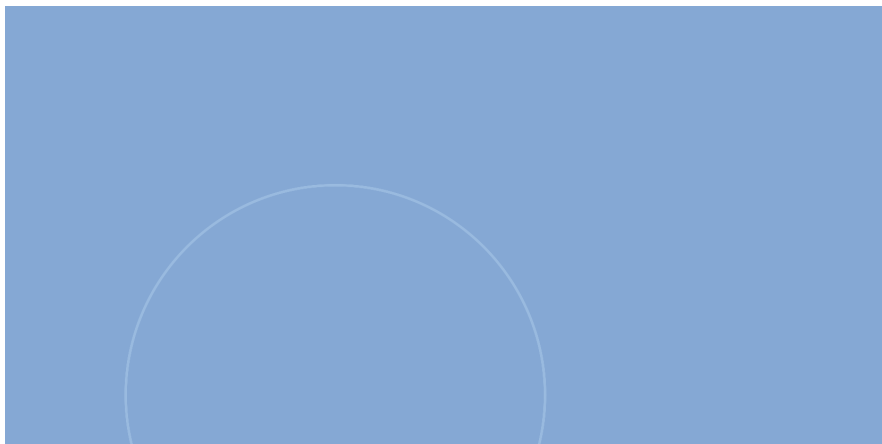
Bibliography

- Akasofu, S., 1964. The development of the auroral substorm. *Planet. Space Sci.* 12, 273–282.
- Akasofu, S., 1981. Energy coupling between the solar wind and the magnetosphere. *Space Sci. Rev.* 28, 121–190.
- Andersson, M., Verronen, P., Rodger, C., Clilverd, M., Seppälä, A., 2014. Missing driver in the sun-earth connection from energetic electron precipitation impacts mesospheric ozone. *Nat. Commun.* 5.
- Appleton, E., 1932. Wireless studies of the ionosphere. *Int. J. Electr. Eng.* 71, 642–650.
- Baker, D., Belian, R., Higbie, P., Hones, E., 1979. High-energy magnetospheric protons and their dependence on geomagnetic and interplanetary conditions. *Jorn. Geophys. Res.* 84, 7138–7154.
- Baker, D., Pulkkinen, T., Angelopoulos, V., Baumjohann, W., McPherron, R., 1996. Neutral line model of substorms: Past results and present view. *Jour. Geophys. Res.* 101.
- Barabash, V., 2004. Investigation of polar mesosphere summer echoes in northern Scandinavia. Ph.D. thesis. Swedish Institute of Space Physics.
- Beharrel, M., Honary, F., Rodger, C., Clilver, M., 2015. Substorm-induced energetic electron precipitation: Morphology and prediction. *JGR Space Physics* 120, 2993–3008.
- Berkey, F., Driatskiy, V., Henriksen, K., Hultqvist, B., Jelly, D., Shchuka, T., Theander, A., Yliniemi, J., 1974. A synoptic investigation of particle precipitation dynamics for 60 substorms in iqsy (1964-1965) and iasy (1969). *Planet. Space Sci.* 22, 255–307.
- Brekke, A., 1997. *Physics of the upper polar.* 2 ed., Springer-verlag.
- Codrescu, M., Fuller-Rowell, T., Roble, R., Evans, D., 1997. Medium energy particle precipitation influences on the mesosphere and lower thermosphere. *JGR Space Phys.* 102.

-
- Cowley, S., 1982. The causes of convection in the earth's magnetosphere: A review of developments during the ims. *Rev. Geophys. Space Phys.* 20, 531–565.
- Cowley, S., 2000. Magnetosphere-ionosphere interactions: A tutorial review. *Magnetospheric current system* 118.
- Cresswell-Moorcock, K., Rodger, C., Kero, A., Collier, A., Clilverd, M., Häggström, I., Pitkänen, T., 2013. A reexamination of latitudinal limits of substorm-produced energetic electron precipitation. *JGR Geophys. Res.* 118, 6694–6705.
- Davis, T., Sugiura, M., 1966. Tauroral electrojet activity index ae and its universal time variations. *Jour. Geophys. Res.* 71.
- Dungey, J., 1961. Interplanetary magnetic field and the auroral zones. *Phys. Rev. Lett.* 6.
- Elphinstone, R., Hearn, D., Cogger, L., Murphree, J., Singer, H., Sergeev, V., Mursula, K., Klumpar, D., Reeves, G., Johnson, M., Ohtani, S., Potemra, T., Sandahl, I., Nielsen, E., Persson, M., Opgenoorth, H., Newell, P., Feldstein, Y., 1995. Observations in the vicinity of substorm onset: Implication for the substorm process. *Jour. Geophys. Res.* 100, 7937–7969.
- Huang, C., Reeves, G., Borovsky, J., Skoug, R., Pu, Z., Le, G., 2003. Periodic magnetospheric substorms and their relationship with solar wind variations. *Jour. Geophys. Res.* 108.
- Hunsucker, R., Hargreaves, J., 2002. *The high-latitude ionosphere and its effect on radio propagation.* Cambridge University Press.
- Juusola, L., Østgaard, N., Tanskanen, E., Partamies, N., Snekvik, K., 2011. Earthward plasma sheet flows during substorm phases. *JGR Space Phys.* 116.
- Kallio, E., Pulkkinen, T., Koskinen, H., Viljanen, A., 2000. Loading-unloading processes in the nightside ionosphere. *Geophys. Res. Lett.* 27, 1627–1630.
- van de Kamp, M., 2013. Harmonic quiet-day curves as magnetometer baselines for ionospheric current analyses. *Geosci. Instrum. Method. Data Syst. Discuss* 3, 87–125.
- Kauristie, K., Pulkkinen, T., Pellinen, R., Opgenoorth, H., 1996. What can we tell about global auroral-electrojet activity from a single meridional magnetometer chain? *Ann. Geophys.* 14, 1177–1185.
- Kero, A., Vierinen, J., McKay-Bukowski, D., Enell, C., Sinor, M., Roininien, L., Ogawa, Y., 2014. Ionospheric electron density profiles inverted from a spectral riometer measurement. *Geophys. Res. Lett.* 41, 5370–5375.
- Kim, H.J., Lee, D.Y., L.R., L., 2008. Are repetitive particle injections during high-speed solar wind streams classic substorms? *Jour. Geophys. Res.* 113.
- Kullen, A., Karlsson, T., 2004. On the relation between solar wind, pseudobreakups, and substorms. *Jour. Geophys. Res.* 109.

-
- Liou, K., Newell, P., Zhang, Y.L., Paxton, L., 2013. Statistical comparison of isolated and non-isolated auroral substorms. *JGR Space Physics* 118, 2466–2477.
- McKay, D., 2018. KAIRA - The Kilpisjärvi Atmospheric Imaging Receiver Array. Ph.D. thesis. The Arctic University Of Norway.
- McPherron, R., 1970. Growth phase of magnetospheric substorms. *Jour. Geophys. Res.* 75, 5592–5599.
- McPherron, R., Chu, X., 2016. Relation of the auroral substorm to the substorm current wedge. *Geosci. Lett.* 3.
- McPherron, R., Russel, C., Aubry, M., 1973. Satellite studies magnetospheric substorms on august 15, 1968. *Jour. Geophys. Res.* 78.
- Mironova, I., Aplin, K., Arnold, F., Bazilevskaya, G., Harrison, R., Krivolutsky, A., Nicoll, K., Rozanov, E., Turunen, E., Usoskin, I., 2015. Energetic particle influence on the earth's atmosphere. *Space Sci. Rev.* 194.
- Nagai, T., 1991. An empirical model of substorm-related magnetic field variations at synchronous orbit. *Magnetospheric substorm, Geophys. Monogr. Ser.* 64, 91–95.
- Newell, P., Gjerloev, J., 2011. Evaluation of supermag auroral electrojet indices as indicators of substorms and auroral power. *JGR Space Physics* 116.
- Oyama, S., Kero, A., Rodget, C., Clilverd, M., Miyoshi, Y., Partamies, N., Turunen, E., Raita, T., Verronen, P., Saito, S., 2017. Energetic electron precipitation and auroral morphology at the substorm recovery phase. *JGR Space Physics* 122.
- Partamies, N., Juusola, L., Tanskanen, E., Kauristie, K., 2013. Statistical properties of substorms during different storm and solar cycle phases. *Ann. Geophys.* 31, 349–358.
- Perreault, P., Akasofu, S.I., 1978. A study of geomagnetic storms. *Geophys. J. R. astr. Soc.* 54, 547–573.
- Pulkkinen, T., Partamies, N., McPherron, R., Henderson, M., Reeves, G., Thomsen, M., Singer, H., 2007. Comparative statistical analysis of storm time activations and sawtooth events. *Jour. Geophys. Res.* 112.
- Reeves, G., Chan, A., Rodger, C., 2009. New directions for radiation belt research. *Space Weather* 7.
- Sandhu, J., Rae, I., Freeman, M., Gkioulidou, M., C., F., Reeves, G., Murphy, K., Walach, M.T., 2018. Substorms - ring current coupling: A comparison of isolated and compound substorms. *JGR Space Physics* 124.
- Seppälä, A., Clilverd, M., Beharrell, M., Rodger, C., Verronen, P., Andersson, M., Newham, D., 2015. Substorm-induced energetic electron precipitation: Impact on atmospheric chemistry 42, 8172–7176.

-
- Siscoe, G., Huan, T., 1985. Polar cap inflation and deflation. *Jour. Geophys. Res.* 90, 543–547.
- Tanskanen, E., 2002. Terrestrial substorms as a part of global energy flow. Ph.D. thesis. Finnish meteorological Institute.
- Turunen, E., Verronen, P., Seppälä, A., Rodger, C., Clilverd, M., Tamminen, J., Enell, C., Ulich, T., 2009. Impact of different energies of precipitating particles on nox generation in the middle and upper atmosphere during geomagnetic storms. *Jour. Atmos. Solar-Terr. Phys.* 71, 1176–1189.
- Wing, S., Gkioulidou, M., Johnson, J., Newell, P.T. Wang, C., 2013. Auroral particle precipitation characterized by the substorm cycle. *JGR Space Physics* 118, 1022–1039.
- Zawdie, K., Drob, D., Siskind, D., Coker, C., 2017. Calculating the absorption of hf radio waves in the ionosphere. *Radio Sci* 52, 767–783.



Norwegian University of
Science and Technology